AMERICAN SOCIETY FOR MICROBIOLOGY | mBio

Check for updates

| Host-Microbial Interactions | Research Article

Forward genetic screen in zebrafish identifies new fungal regulators that limit host-protective *Candida*-innate immune interaction

Bailey A. Blair,[1,2] Emma Bragdon,[1] Gursimran Dhillon,[1] Nnamdi Baker,[1] Lena Stasiak,[1] Mya Muthig,[1] Pedro Miramon,[3] Michael C. Lorenz,[3] Robert T. Wheeler[1,2]

AUTHOR AFFILIATIONS See affiliation list on p. 21.

ABSTRACT *Candida* is one of the most frequent causes of bloodstream infections, and our first line of defense against these invasive infections is the innate immune system. The early immune response is critical in controlling *Candida albicans* infection, but *C. albicans* has several strategies to evade host immune attack. Phagocytosis of *C. albicans* blocks hyphal growth, limiting host damage and virulence, but how *C. albicans* limits early recruitment and phagocytosis in vertebrate infection is poorly understood. To study innate immune evasion by intravital imaging, we utilized the transparent larval zebrafish infection model to screen 131 *C. albicans* mutants for altered virulence and phagocyte response. Infections with each of the seven hypovirulent mutants led to altered phagocyte recruitment and/or phagocytosis, falling into four categories. Of particular interest among these is *NMD5*, a predicted β-importin and newly identified virulence factor. The *nmd5*Δ/Δ mutant fails to limit phagocytosis, and its virulence defects are eliminated when phagocyte activity is compromised, suggesting that its role in virulence is limited to immune evasion. These quantitative intravital imaging experiments are the first to document altered *Candida*–phagocyte interactions for several additional mutants and clearly distinguish recruitment from phagocytic uptake, suggesting that *Candida* modulates both events. This initial large-scale screen of individual *C. albicans* mutants in a vertebrate, coupled with high-resolution imaging of *Candida*–phagocyte interactions, provides a more nuanced view of how diverse mutations can lead to more effective phagocytosis, a key immune process that blocks germination and drives anti-fungal immunity.

IMPORTANCE *Candida albicans* is part of the human microbial community and is a dangerous opportunistic pathogen, able to prevent its elimination by the host immune system. Although *Candida* avoids immune attack through several strategies, we still understand little about how it regulates when immune phagocytes get recruited to the infection site and when they engulf fungal cells. We tested over 130 selected *Candida* mutants for their ability to cause lethal infection and found several hypovirulent mutants, which provoked altered innate immune responses, resulting in lower overall inflammation and greater host survival. Of particular interest is *NMD5*, which acts to limit fungal phagocytosis and is predicted to regulate the activity of stress-associated transcription factors. Our high-content screening was enabled by modeling *Candida* infection in transparent vertebrate zebrafish larva. Our findings help us understand how *Candida* survives immune attack during commensal and pathogenic growth, and may eventually inform new strategies for controlling disease.

KEYWORDS *Candida*, innate immunity, phagocytosis, macrophages, neutrophils, virulence determinants, immune evasion, zebrafish

Editor J. Andrew Alspaugh, Duke University Hospital, Durham, North Carolina, USA

Address correspondence to Robert T. Wheeler, robert.wheeler1@maine.edu.

The authors declare no conflict of interest.

See the funding table on p. 22.

Received 25 February 2025
Accepted 27 February 2025
Published 2 April 2025

Candida albicans is one of the most common bloodstream infections in the United States, causing approximately 25,000 cases annually (CDC). *C. albicans* can normally be found as a commensal in the gastrointestinal tract, mouth, skin, or vagina in up to 70% of the population (1–3). While *C. albicans* is found in healthy individuals, it can also cause infections ranging from superficial mucosal infections such as vulvovaginal candidiasis and oropharyngeal candidiasis to lethal systemic infections with attributable mortality rates of approximately 25% (4, 5). The host immune response is tasked with protecting individuals from these infections, with the innate immune system being of special importance in fighting systemic *Candida* infections. In turn, *C. albicans* employs many mechanisms to subvert the actions of the host immune attack (6–14). While we understand some of how *C. albicans* can evade host immune responses *in vitro*, we still know little about this during vertebrate infection.

The innate immune response is the first line of defense against *C. albicans* and is critical in controlling and preventing systemic candidiasis (15–19). This is highlighted by the fact that patients with neutropenia are more susceptible to invasive *Candida* infections, and mice with macrophage defects survive experimental systemic infection poorly. Phagocytes get to the infection site by following cytokine and chemokine gradients and presumably identify fungal cells for ingestion using fungal-derived chemoattractants (17, 18, 20). While phagocytes play crucial roles, other innate immune cells such as epithelial cells, microglia, natural killer cells, and innate lymphocytes also play important roles (18, 21). Cytokines and chemokines, which bring phagocytes to the infection site, simultaneously activate them and induce their differentiation. Once there, phagocytes must locate fungal cells by soluble cues, recognize the foreign microbial cells based on surface patterns and opsonins, and initiate phagocytosis.

Immune cells such as phagocytes recognize pathogen-associated molecular patterns (PAMPs) in *C. albicans* cell wall, but *C. albicans* is able to shield them from immune cells behind a layer of mannosylated proteins of the outer cell wall (9). Macrophages and neutrophils are the main effector cells against *C. albicans* and employ many strategies to kill *C. albicans*. These cells are able to phagocytose *C. albicans* yeast as well as short hyphae, produce antimicrobial peptides, reactive oxygen species, and extracellular traps to combat *C. albicans* (8, 13, 14, 22). Not only can *C. albicans* shield its cell wall PAMPs from these cells, but once taken up by a phagocyte, *C. albicans* can survive by preventing the fusion of the phagosome with the lysosome, alkanizing the acidic environment of the phagolysosome, producing catalase and superoxide dismutase to counteract ROS, and upregulating DNA repair systems and heat shock proteins to counteract damage caused to DNA and proteins (23, 24). In addition, *C. albicans* has also been seen to escape from host cells such as macrophages by inducing pyroptosis; or also, although rare, vomocytosis (23, 25). These mechanisms were initially described *in vitro*, yet we still do not fully understand which mechanisms play critical roles during infection or which fungal pathways mediate these activities.

The larval zebrafish provides a unique model that is well suited to investigate the interactions between *C. albicans* and the vertebrate innate immune response (26–28). The transparency and availability of many transgenic lines permit quantitative imaging of the immune response to *C. albicans* infection in the context of a live host. Furthermore, the small size and fertility of zebrafish enable cost-effective, moderate- to high-throughput screening in a vertebrate model. Previous results suggest that the early phagocyte response is critical to survive a *C. albicans* hindbrain ventricle infection (29, 30). Evidence from the larval zebrafish also suggests that *C. albicans* has the ability to limit this response by reducing the recruitment of phagocytes to the infection site (30). This ability to limit phagocyte recruitment was observed for a wild-type (WT) *C. albicans* strain, but not a yeast-locked strain, suggesting this response may be regulated with the yeast to hyphal transition.

We sought to identify new *C. albicans* factors playing a role in limiting early phagocyte responses by leveraging the transparent zebrafish infection model. Because virulence is linked to early phagocytic efficiency, we screened 131 engineered *C. albicans* mutants for

virulence defects in the larval zebrafish hindbrain infection model. As there may be links between evasion of phagocyte recruitment and the yeast-to-hyphal transition, we chose a set of mutants that had been characterized in a previous high-throughput pooled screen as having either an infectivity defect only or a morphogenesis defect only (31). Because little is known about soluble chemoattractants secreted by *Candida*, we also included single mutants from groups of genes that code for potential secreted proteins such as secreted aspartyl proteases and lipases. Mutations that were associated with hypovirulence and could be faithfully complemented were then screened for multiple phagocyte recruitment and phagocytosis phenotypes during early infection. Several genes previously known to alter morphology and/or virulence were found to limit early phagocytosis of *Candida*, a previously unknown function of these genes. Strikingly, the predicted karyopherin *NMD5* lost its virulence defect when the host was immunosuppressed in any of three ways—suggesting that its role in virulence is largely confined to limiting early phagocyte recruitment and phagocytosis. These results expand our understanding of how *Candida* virulence genes mediate pathogenesis through limiting the early innate immune response.

RESULTS

Forward genetic screen for altered fungal immune evasion based on loss of virulence

C. albicans is known to limit immune recruitment and phagocytosis during infection; although morphological switching can regulate phagocyte recruitment, few molecular details are known about how this occurs (30, 32, 33). The zebrafish hindbrain infection model provides a useful *in vivo* system to intravitally image early fungal and host dynamics, and has identified a close correlation between early phagocyte-mediated fungal containment and overall survival (29, 30, 33). We leveraged these advantages to screen individual *C. albicans* mutants for virulence and phagocytosis defects, with an initial screen for hypovirulence and a secondary screen for altered fungal–phagocyte interaction.

We used a small number of mutants to define infection parameters and enable high-throughput screening; these mutants have normal *in vitro* competitive fitness, were present in our strain collections, and are predicted to have cell wall defects (*mnn15*Δ/Δ, *mnt1*Δ/Δ), known to have filamentous growth defects or altered interaction with phagocytes *in vitro* (*mad2*Δ/Δ, *ece1*Δ/Δ, *pra1*Δ/Δ), and/or hypovirulence in murine models (Table S1) (34–37). In initial virulence tests, two mutant strains were tested along with controls, and at least three biologically independent experiments were performed with approximately 50 fish infected per mutant (Fig. 1A). Inocula were counted by fluorescence microscopy to ensure they received the correct amount of *Candida* (10–25 fungal cells), then larvae were followed for survival for 3 days relative to the SN250 wild type (Fig. 1B). Three of the nine strains tested had significantly reduced (*ssu81*Δ/Δ and *mad2*Δ/Δ) or abolished virulence (*rbt1*Δ/Δ$^{968\text{-}2166}$) (Fig. 1C). We then used the average and standard deviation (SD) of 72 hours postinfection (hpi) survival for wild-type-infected fish to determine z-score cutoffs for subsequent experiments, to exclude data in which wild-type-infected survival was out of range (average ±2.5 SD [20%–80% survival]). In addition, we quantified host–pathogen interactions by confocal microscopy at 4–6 hpi, scoring fungal cells as intra- versus extra-cellular based on a combination of Calcofluor white staining of the inoculum and differential interference contrast (DIC) imaging of host phagocytes (Fig. 1D insets and 1E). Although this method was limited because only the initial inoculum was fluorescently stained and phagocytes were not fluorescent, there was a consistent trend for increased fungal phagocytosis of *mad2*Δ/Δ compared to the control SN250 (Fig. 1E; Table S2, $P = 0.009$, effect size = 0.90; large). The *rbt4*Δ/Δ mutant was phagocytosed significantly less efficiently ($P = 0.029$, effect size = 0.55; large) but was not pursued further because the lower phagocytosis was not associated with altered survival (Fig. 1C). Interestingly, *mad2*Δ/Δ was also one of the three strains with significantly reduced virulence (Fig. 1B and C). The other two hypovirulent mutants failed

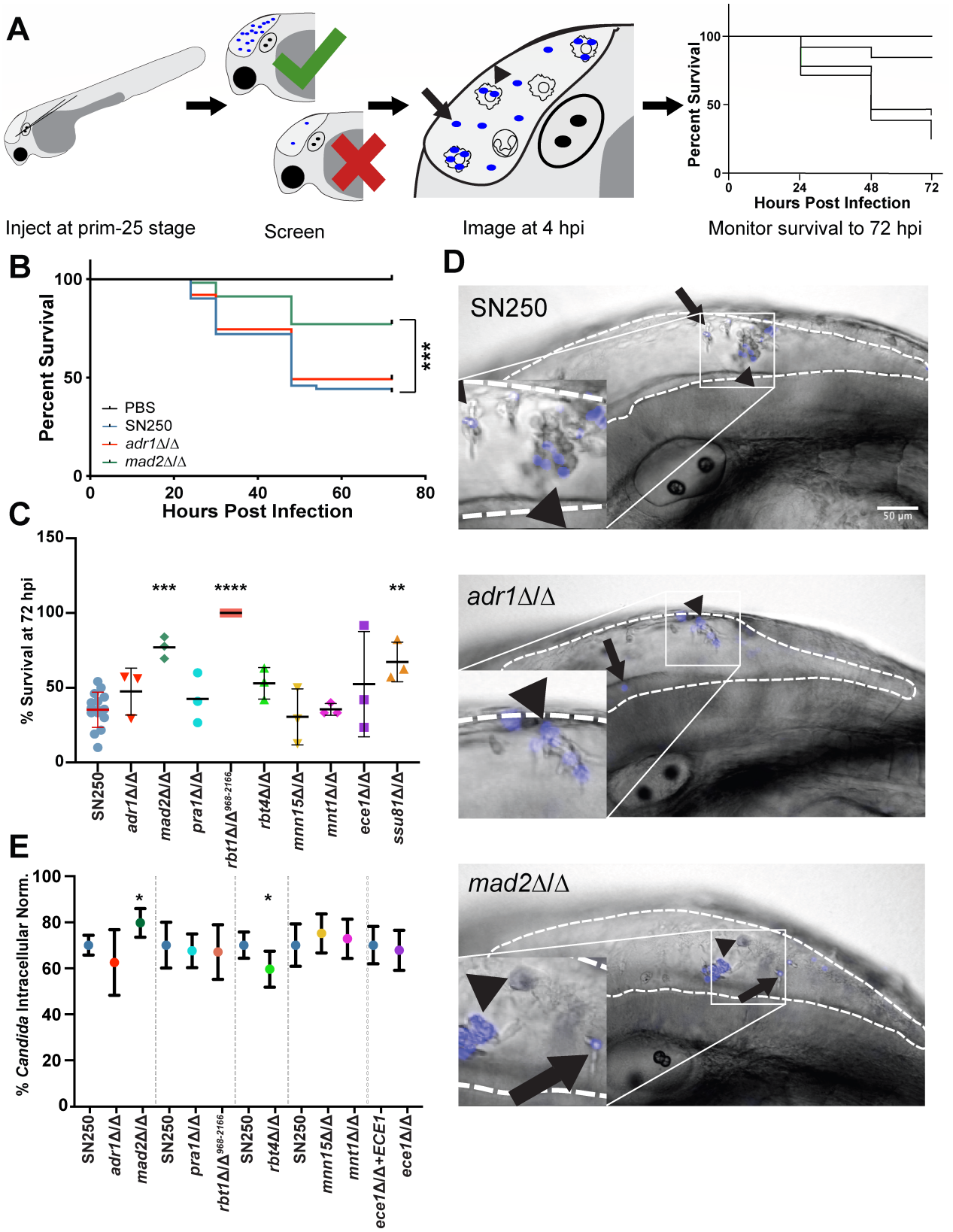

FIG 1 Defining infection parameters. (A) Flow chart showing the workflow of pilot experiments. Hindbrain infections were performed at the prim-25 stage, and fish were then screened to ensure they received the correct inoculum (10–25 cells). At 4–6 hours postinfection, fish were imaged by confocal microscopy to score fungal phagocytosis; survival was monitored out to 72 hpi. (B) Example Kaplan-Meier survival curves pooled from three experiments showing the

(Continued on next page)

Fig 1 (Continued)

fish injected with PBS (control, *n* = 83), SN250 (WT, *n* = 61), *adr1*Δ/Δ (*n* = 63), or *mad2*Δ/Δ (*n* = 57). Fish injected with *mad2*Δ/Δ showed increased survival compared to SN250 (*P* = 0.0001). (C) Survival of fish injected with each strain at 72 hpi in three independent experiments. Individual points represent biologically independent experiments on different days. Bars show means and standard deviations with SN250 in red to depict WT cutoff range for inclusion of experiments. Significant differences in survival curves were determined by Mantel-Cox log-rank tests comparing the mutant strain to SN250 from data pooled from three biological replicates of the same experiments. Two mutants were tested per experiment, and Bonferroni corrections were performed. (D) Representative images of hindbrain ventricle infection to score fungal phagocytosis at 4 hpi. *C. albicans* initial inoculum was stained with Calcofluor white, shown in blue. The hindbrain ventricle is outlined by white dashed lines. Scalebar is 50 µm. Arrows point to extracellular *Candida*, while arrowheads point to intracellular *Candida*. (E) Quantification of the percent of intracellular *Candida*. Fungal cells were scored as intracellular or extracellular from z-stack slices (using Calcofluor fluorescence for the fungi and differential interference contrast [DIC] for imaging the phagocytes) of individual fish taken at 4–6 hpi for each strain. Based on at least 19 fish from at least three independent experiments. Significance and effect size were determined as described in Materials and Methods and based on reference 38. **P* < 0.05, ***P* < 0.01, ****P* < 0.001.

later validation steps—*rbt1*Δ/Δ$^{968\text{-}2166}$ failed at the complementation step, and *ssu81*Δ/Δ failed when the second isolate was tested. Although morphological quantification of the fungi was not possible because only the inoculum was labeled, and the inoculum was all yeast cells for all strains, there were no qualitative differences noted in the amount of filamentous growth (as visualized by brightfield microscopy) between SN250 and any of the mutant strains.

A total of 131 mutant *C. albicans* strains with expected deficiencies in predicted secreted factors, hyphal growth, or virulence were then selected for screening (Table S1), based on their phenotypes observed in previous screens (31). One group of strains (the Morphology category) was selected for a published defect in hyphal growth on Spider medium but no defect in virulence, as we hypothesized that these mutants might disrupt the co-regulation of immune evasion mechanisms with the yeast-to-hyphal transition (10). While these strains have a morphogenesis defect on Spider plates, defects in filamentous growth are often very dependent on the environmental context and strain, and therefore may or may not have a filamentous growth defect in the zebrafish hindbrain (39–41). A complementary set of strains (the Infectivity category) had a competitive defect in pooled mouse infection but no morphogenesis defect on Spider agar; we reasoned these strains may be cleared more effectively by the host immune response even if they are not defective in filamentous growth. This included 69 mutants that had a morphogenesis defect on Spider agar but no pooled virulence defect, 41 that had an infectivity defect in pooled infection but no Spider morphogenesis defect, and one that had both defects. The final category (Secreted-Predicted) included 20 genes encoding predicted secreted peptides—including lipases, proteases, and other genes annotated as potentially secreted—but the mutants had no Spider agar morphogenesis or pooled virulence defect (31) (Table S1).

In this primary screen, we chose to facilitate high-throughput screening for cell-autonomous virulence defects, so inocula were not counted and no replicates were performed. Virulence testing revealed several mutants with greatly reduced virulence, as measured by z-score (based on deviance from the mean for WT infection, see Materials and Methods). Seventeen had a fish survival z-score >3, while 27 had a z-score between 2 and 3 (Fig. 2). Of the 41 strains in the Infectivity category, six of these had a z-score >3, with another six between z-scores of 2 and 3. Out of the 70 in the Morphogenesis category, 11 had a z-score >3, with another 16 between 2 and 3. In addition, four genes from the secreted aspartyl protease (SAP) family of genes had z-scores between 2 and 3. As these fish were not screened to ensure the correct number of *C. albicans* injected (10–25 fungal cells), we first retested hypovirulent strains with z-scores >3 with an added step of screening for inoculum per fish. On retest, both independent isolates from the Noble library were tested, and strains were genotyped to confirm the correct gene deletion. After retesting, this led to a total of 10 mutants with reproducible hypovirulence: *rbt1*Δ/Δ$^{968\text{-}2166}$, *orf19.5547*Δ/Δ, *pep8*Δ/Δ, *cht2*Δ/Δ, *apm1*Δ/Δ, *rim101*Δ/Δ, *brg1*Δ/Δ, *nmd5*Δ/Δ, *mad2*Δ/Δ, and *cek1*Δ/Δ (Table S1). Hypovirulent strains were then

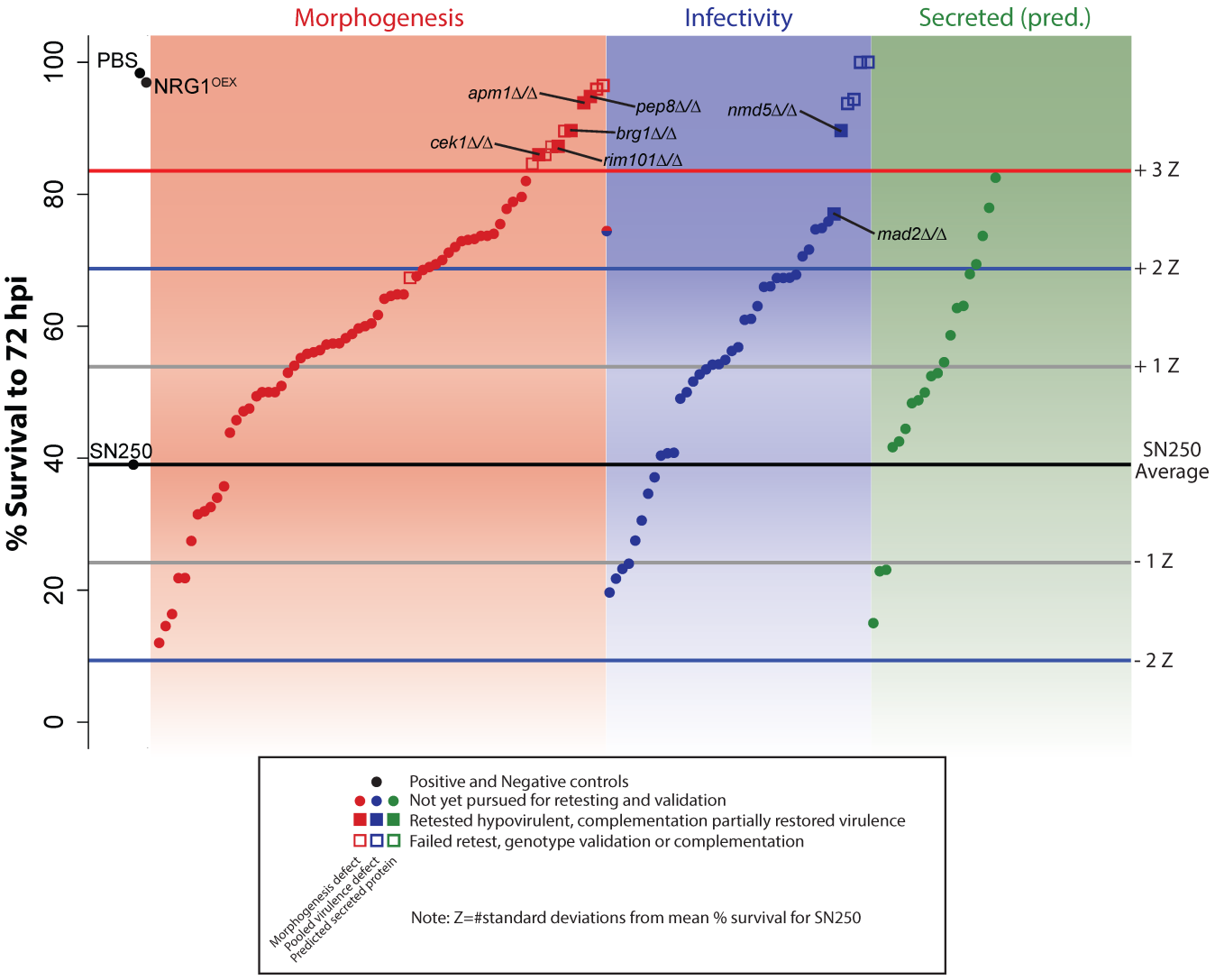

FIG 2 High-throughput virulence screening. Average survival of fish infected with individual mutant *C. albicans* strains ($n \approx 50$ fish per mutant strain). Mock-infected (PBS) and NRG1^{OEX}-infected fish were included as controls. The average survival of the WT SN250 strain is shown by the black line, while differential survival was measured by z-score (based on the standard deviation of % survival in over 20 experiments with SN250 control infections). Gray lines show a z-score = 1, blue lines show a z-score = 2, and red, a z-score = 3. Strains in the red panel were previously seen to have a morphogenesis defect on Spider agar, while those in the blue panel showed a defect in pooled virulence tests, and those in the green panel code for predicted secreted proteins. Mutant strains that had a z-score of over 3 were passed to the next phase of screening, shown as squares. Strains in which both independent mutants showed hypovirulence had their genotypes PCR-confirmed and in which complementation restored virulence are shown as filled squares and were passed to the imaging phase of screening. Those that did not pass secondary screening are shown as empty squares. Complete data are found in Table S1.

complemented to assess if complementation restored virulence. When available, *in vitro* phenotypes (e.g., morphogenesis defect on Spider media) were also used to assess functional complementation of strains prior to assessing virulence in hindbrain infection. Complementation successfully restored at least some virulence to *brg1*Δ/Δ, *pep8*Δ/Δ, *nmd5*Δ/Δ, *rim101*Δ/Δ, *cek1*Δ/Δ, *apm1*Δ/Δ, and *mad2*Δ/Δ mutants (Fig. 3). It also partially restored *in vitro* filamentous growth and pH-dependent filamentation phenotypes for *brg1*Δ/Δ, *pep8*Δ/Δ, and *rim101*Δ/Δ (Fig. S1). We were not able to generate complemented strains that restored even partial virulence to *cht2*Δ/Δ, *orf19.5547*Δ/Δ, or *rbt1*Δ/Δ$^{968\text{-}2166}$ (Fig. S2A through C). Consistent with the failure to complement the partial open reading frame (ORF) deletion in *RBT1*, an independently created full deletion of *RBT1* in the SN250 background did not cause a virulence defect (Fig. S2D). The failure to complement the

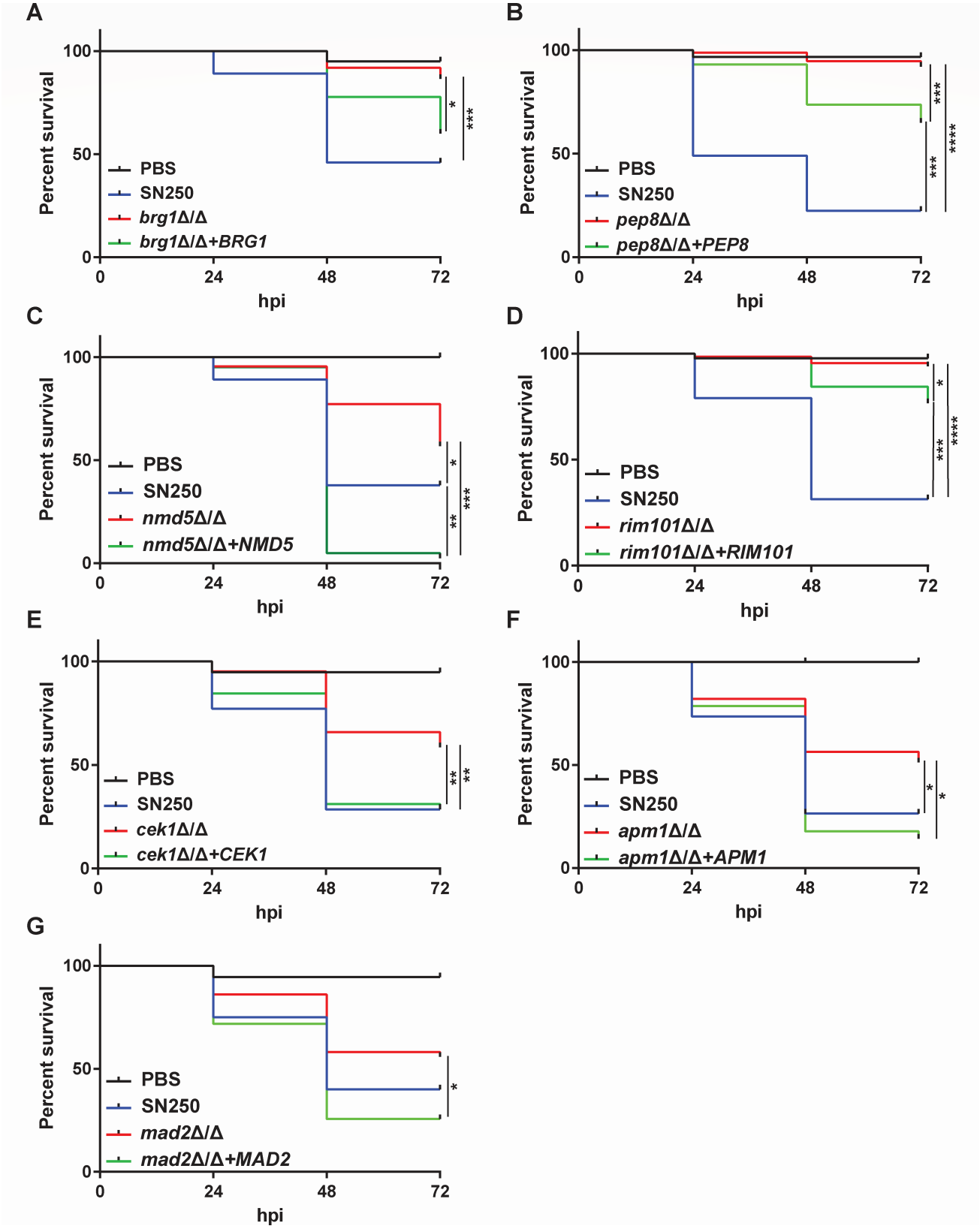

FIG 3 Complementation restores virulence to hypovirulent *C. albicans* mutants. Kaplan-Meier survival curves show restoration of virulence with complementation. All data in survival curves are pooled from two experiments unless otherwise noted. (A) Fish injected with SN250 (WT, n = 37), *brg1*Δ/Δ (n = 37), *brg1*Δ/Δ+*BRG1* (n = 45), PBS (mock, n = 20). Complementation of *brg1*Δ/Δ restores some virulence. (B) Fish injected with SN250 (WT, n = 49), *pep8*Δ/Δ (n = 75),

(Continued on next page)

Fig 3 (Continued)

*pep8*Δ/Δ+*PEP8* (*n* = 57), or PBS (mock, *n* = 30). Complementation of *pep8*Δ/Δ restores some virulence (data pooled from three experiments). (C) Fish injected with PBS (mock, *n* = 20), SN250 (WT, *n* = 37), *nmd5*Δ/Δ (*n* = 44), *nmd5*Δ/Δ+NMD5 (*n* = 41). Complementation significantly increases virulence of *nmd5*Δ/Δ. (D) Fish injected with SN250 (WT, *n* = 45), *rim101*Δ/Δ (*n* = 43), *rim101*Δ/Δ+*RIM101* (*n* = 41), or mock-infected fish (PBS, *n* = 20). Complementation of *rim101*Δ/Δ restores virulence (data pooled from three independent experiments). (E) Fish injected with SN250 (WT, *n* = 35), *cek1*Δ/Δ (*n* = 41), *cek1*Δ/Δ+*CEK1* (*n* = 45), or mock-infected fish (PBS, *n* = 19). Complementation of *cek1*Δ/Δ restores virulence. (F) Fish injected with PBS (mock, *n* = 21), SN250 (WT, *n* = 34), *apm1*Δ/Δ (*n* = 39), or *apm1*Δ/Δ+*APM1* (*n* = 28). Complementation significantly increases virulence of *apm1*Δ/Δ. (G) Fish injected with PBS (mock, *n* = 18), SN250 (WT, *n* = 40), *mad2*Δ/Δ (*n* = 43), or *mad2*Δ/Δ+*MAD2* (*n* = 39). Complementation significantly increases virulence of *mad2*Δ/Δ. *$P_{adj} < 0.05$, **$P_{adj} < 0.01$, ***$P_{adj} < 0.001$, ****$P_{adj} < 0.0001$.

virulence defects in these strains with the full-length gene suggests that the virulence defect is due to other, non-targeted, genomic changes sustained during their original construction. Mutants that could be complemented were then transformed with pENO1-iRFP (42) to drive cytosolic expression of a near-infrared fluorescent protein for intravital imaging of infections. At the conclusion of this first part of the screen, we were left with seven mutants whose virulence defects could be at least partially complemented with add-back of a full-length copy of the gene: five in the Morphogenesis class (*brg1*Δ/Δ, *pep8*Δ/Δ, *rim101*Δ/Δ, *apm1*Δ/Δ, and *cek1*Δ/Δ), two in the Infectivity class (*nmd5*Δ/Δ and *mad2*Δ/Δ), and none in the Predicted Secreted class.

Altered early phagocyte responses to hypovirulent *Candida* mutants

Previous work has linked efficient early immune phagocytosis of fungi to enhanced survival (29, 30). To determine if the virulence defects for these mutants were associated with a more effective early immune response, we imaged *Tg(mpeg1:GFP)/(lysC:dsRed)* larvae (green macrophages and red neutrophils) infected with iRFP-expressing *Candida* at 4–6 hpi. From these images, we assessed the number of macrophages and neutrophils responding rapidly to infection as well as their ability to phagocytose *Candida*, as measured by the number of extracellular fungi, percent phagocytosis, and the number of fungi/recruited phagocyte. We chose these measures to quantify (i) the overall ability of phagocytes to internalize fungi, keep them internalized, and prevent their extracellular proliferation; (ii) the relative efficiency of phagocytosis, without consideration of the total number of extracellular cells, indicating the overall capacity of recruited phagocytes to engulf fungi; and (iii) the average ability of any given phagocyte at the infection site to engulf fungi, providing an indicator of the activation state of the phagocytes and their ability to identify and engulf fungi.

Overall, we found altered acute immune responses to each of the seven validated hypovirulent mutants, with mutant phenotypes in four groups based on infection site immune cell counts and phagocytosis efficiency at 4–6 hpi (Fig. 4). Three mutants in Group I (*mad2*Δ/Δ, *rim101*Δ/Δ, and *brg1*Δ/Δ) were phagocytosed more effectively, and there were lower phagocyte numbers at the infection site at 4–6 hpi. Two mutants in Group II (*pep8*Δ/Δ and *apm1*Δ/Δ) had unchanged phagocytosis efficiency and fewer immune cells. One (Group III; *nmd5*Δ/Δ) had greater phagocytosis with an unchanged phagocyte number, and one (Group IV; *cek1*Δ/Δ) had increased phagocytosis and an increased phagocyte count. The phenotypic scoring is described below in more detail.

Mutants in Groups I, II, and IV had altered numbers of phagocytes at the infection site at 4–6 hpi, as evidenced by comparisons with wild-type infections (Fig. 5 ; *P* values and effect sizes are summarized in Fig. 4 and detailed in Table S3; see Materials and Methods). Infections with the *cek1*Δ/Δ mutant elicited a higher number of total phagocytes and macrophages (*P* values 0.13, 0.14; effect sizes moderate 0.43, 0.41). In contrast, there was a lower number of macrophages at the infection site in *brg1*Δ/Δ and *pep8*Δ/Δ infections (*P* values 0.01, 0.10; effect sizes large, 0.69, or moderate, 0.47) and a lower number of neutrophils in *mad2*Δ/Δ, *rim101*Δ/Δ, and *pep8*Δ/Δ infections (*P* values 0.066, 0.113, 0.046; effect sizes moderate, 0.44, 0.45, or large, 0.59). The small number of neutrophils present early during infection (often zero) suggests that they usually play a limited role early on,

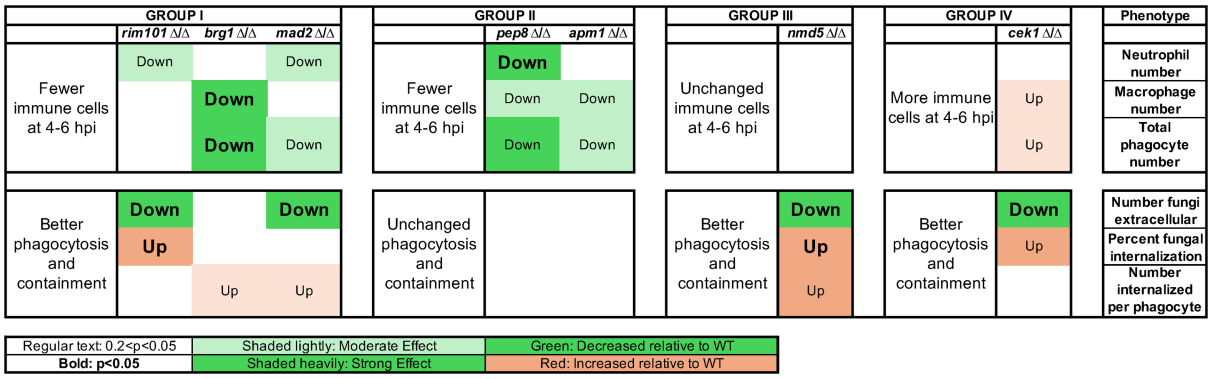

FIG 4 Mutants grouped by altered innate immune response. Mutant–phagocyte interactions were scored at 4–6 hpi, relative to wild-type fungi–phagocyte interactions in the same experiment, as to immune cell number and phagocytosis efficiency traits. Group I mutants had lower numbers of recruited phagocytes and better phagocytosis and containment. Group II mutants had fewer recruited phagocytes and unchanged phagocytosis efficiency. The Group III mutant had no change in phagocyte recruitment but better phagocytosis. The Group IV mutant had higher phagocyte recruitment and better phagocytosis. "Down" or "up" text indicates the direction of differential immune response, bold lettering indicates $P < 0.05$, and regular lettering indicates $0.2 < P < 0.05$. Heavy shading indicates strong effect size; light shading indicates moderate effect size.

so differential neutrophil recruitment likely has more muted biological consequences. Taken together, these data suggest that there is overall decreased phagocyte recruitment to infections with the Group I (*mad2*Δ/Δ, *rim101*Δ/Δ, *brg1*Δ/Δ) and Group II (*pep8*Δ/Δ and *apm1*Δ/Δ) mutants, and overall increased phagocyte recruitment to *cek1*Δ/Δ (Group IV).

The ability of phagocytes to engulf fungi—and thereby limit filamentous growth and contain the infection—within the first few hours is associated closely with overall survival of a wild-type infection (29, 30). Mutants in Groups I, III, and IV had an overall increase in the ability of phagocytes to internalize fungi. Zebrafish infected with *nmd5*Δ/Δ (Group III) were more effective at each of these measures of fungal internalization (Table S3; Fig. 4 and Fig. 6), with a higher percent internalization (*P* value 0.009; large effect size 0.69) and number of fungi per phagocyte (*P* value 0.05; large effect size 0.55) and a lower number of extracellular fungi (*P* value 0.02; large effect size 0.65). Fish infected with Group I and IV mutants (*mad2*Δ/Δ, *rim101*Δ/Δ, *brg1*Δ/Δ, and *cek1*Δ/Δ) also exhibited at least one measure of increased fungal phagocytosis with at least a moderate effect size (Table S3; Fig. 4 and Fig. 6). Overall, the phagocyte response was able to internalize each of the hypovirulent mutants at least as well as the wild-type strain in the first 4–6 hpi, with five of the seven mutants phagocytosed more effectively than wild type. This is consistent with the original premise of the screen, which was designed to identify mutants with reduced capacity to avoid innate phagocyte attack by screening initially for hypovirulence.

Fungal morphology defects of mutants early during infection do not correlate with altered innate immune responses

Because filaments are more difficult to phagocytose than yeast, and five of the seven hypovirulent mutants had been previously identified as having filamentous growth phenotypes on Spider agar, we sought to determine if they also had problems switching to filamentous morphology *in vivo* in the first few hours of infection (31, 43–46). We imaged hindbrain infections with each mutant and analyzed the amount of yeast-shaped vs elongated cells at 4–6 hpi, as cells switching to filamentous growth would have had time to grow longer but would not yet have a hyphal shape (Fig. S3A). Not unexpectedly, four of the five mutants with reduced *in vitro* filamentation (*rim101*Δ/Δ, *brg1*Δ/Δ, *pep8*Δ/Δ, and *apm1*Δ/Δ, but not *cek1*Δ/Δ) had a reduced number of elongated cells *in vivo* at this early time point, with dramatic defects in the *rim101*Δ/Δ, *brg1*Δ/Δ, and *pep8*Δ/Δ mutants (Fig. S3B; Fig. 7, n.b. effect size in table indicated only for those comparisons with $P < 0.05$). On the other hand, neither *cek1*Δ/Δ nor the two mutants in the Infectivity class

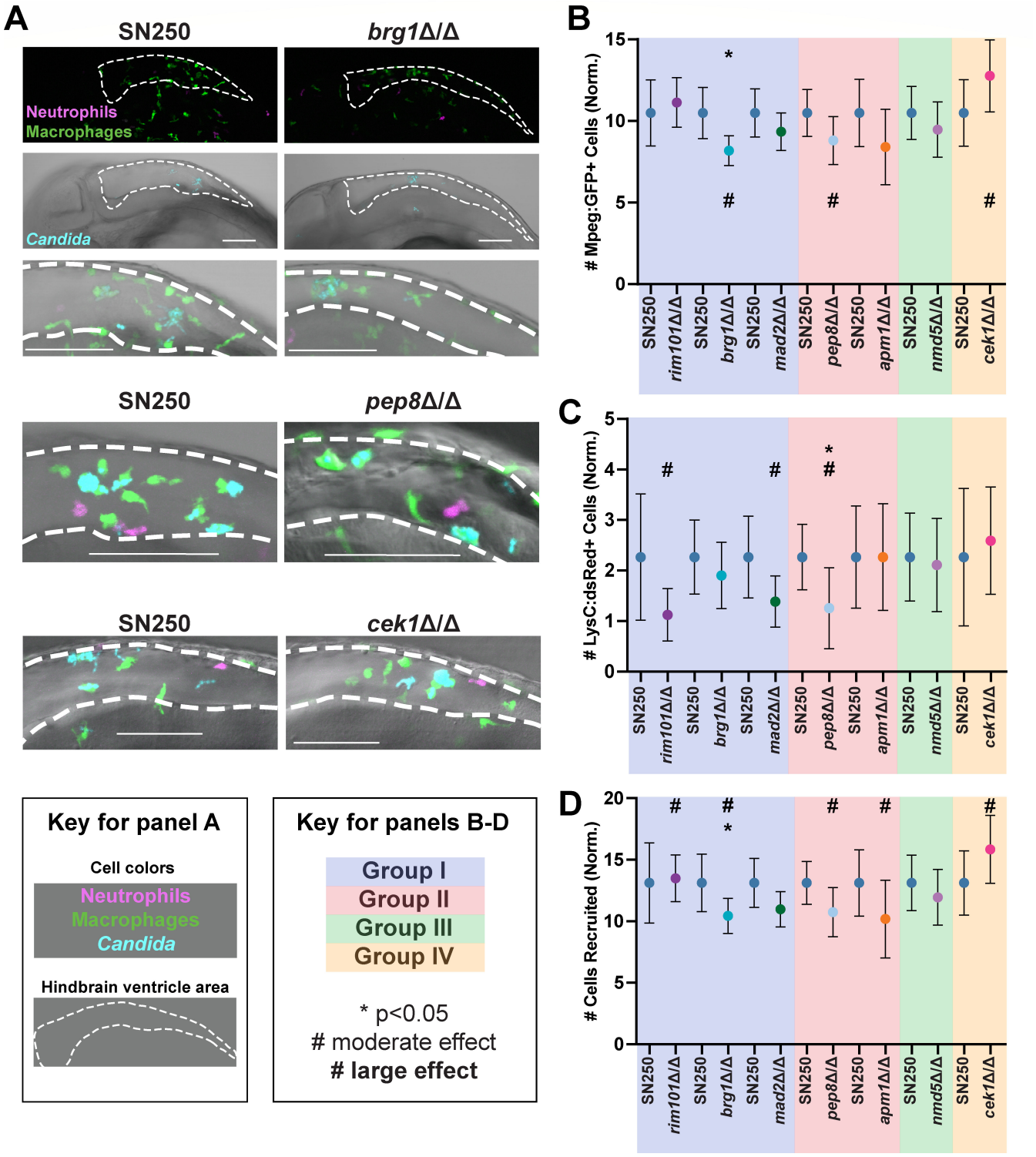

FIG 5 Phagocyte recruitment to hypovirulent *C. albicans* mutants. (A) Example representative images from *brg1*Δ/Δ, *pep8*Δ/Δ and *cek1*Δ/Δ-infected fish, along with SN250-infected controls, at 4–6 hours postinfection. Images were scored by eye for the number of macrophages (*mpeg1*:GFP+ cells) shown in green and the number of neutrophils (*lysC*:dsRed+ cells) in magenta recruited to the infection, as well as if the *Candida* was intracellular or extracellular. Scale bar is 100 µm. (B–D) Quantification of phagocyte recruitment-related phenotypes. There are separate SN250 columns for each set of experiments, as the mutant was compared to wild type in the same experiments. (B) Plots showing the number of *mpeg*:GFP+ macrophages recruited to the infection site normalized to the average amount of *mpeg*:GFP+ macrophages recruited to SN250. (C) Plots showing the number of *lysC*:dsRed+ neutrophils recruited to the infection site normalized to the average amount of *lysC*:dsRed+ neutrophils recruited to SN250. (D) Plots showing the number of cells recruited to the infection site normalized to the

(Continued on next page)

Fig 5 (Continued)

average recruited to SN250. Cells include *mpeg1*:GFP+ and *lysC*:dsRed+ cells recruited to the hindbrain, as well as non-fluorescent cells containing *Candida*. (B–D) Shading indicates Groups I–IV based on similar interaction phenotypes (Fig. 4). Means and 95% confidence intervals are plotted. Statistics were performed from data pooled from at least three independent experiments for each mutant, for approximately 25 fish per strain were imaged. Hedges bias-corrected effect sizes and significance were determined for each mutant. * indicates $P < 0.05$, # indicates a moderate effect, while a bold # indicates a strong effect.

of mutants (*nmd5*Δ/Δ and *mad2*Δ/Δ) had a significant reduction in filamentous growth. Early phagocytosis is associated with inhibition of germination and lower virulence (29, 30), which could be a factor in reduced filamentous growth. However, because *rim101*Δ/Δ was the only one of the four mutants with reduced filamentous growth that was phagocytosed at a higher rate, this suggests that the other three mutants form fewer filaments *in vivo* because they have an intrinsically reduced ability to switch to filamentous growth during infection. Interestingly, there was no concordance between significantly altered innate immune responses (in recruitment or phagocytosis efficiency) and a reduced ability to switch to filamentous growth in the early hours of infection. For instance, *mad2*Δ/Δ and *rim101*Δ/Δ have very similar phagocyte response profiles (Fig. 4, Group I), but only *rim101*Δ/Δ has a strong and significant morphogenesis defect at this early time point *in vivo* (Fig. 7).

Altered cytokine responses to hypovirulent *Candida* mutants

We reasoned that these altered immune responses might be accompanied by altered expression of proinflammatory cytokines and chemokines. Because immune recruitment and phagocytosis were altered most profoundly for the *brg1*Δ/Δ, *pep8*Δ/Δ, and *nmd5*Δ/Δ mutants, and they belong to different classes of mutants (Fig. 4), we chose to measure inflammatory gene induction in these infections. We measured the expression of two key proinflammatory cytokines (interleukin-1 beta and tumor necrosis factor alpha) and the zebrafish IL-8 homolog, each of which is associated with response to *Candida* infection (47). At 4 hpi, there was not a significant induction of pro-inflammatory gene expression (Fig. S4), but there was a robust induction of these genes by 24 hpi (Fig. 8). At 24 hpi, fish infected with *brg1*Δ/Δ or *pep8*Δ/Δ showed a significant reduction in *cxcl8b*, *tnfa*, and *il1b* induction, while fish infected with *nmd5*Δ/Δ showed a significant reduction in *cxcl8b* and *il1b* induction but not *tnfa* (Fig. 8A through C). Fish infected with *nmd5*Δ/Δ+*NMD5* showed a trend for increased proinflammatory chemokine/cytokine production, even compared to SN250, which reached significance for *il1b*. This matches well with the decreased survival of fish infected with this complemented strain and the complete complementation phenotype (Fig. 3C). On the other hand, *cxcl8b*, *tnfa*, and *il1b* expression for *brg1*Δ/Δ+*BRG1* and *pep8*Δ/Δ+*PEP8* tended to be between SN250 and the mutant strain, which matches the partial complementation of virulence exhibited by these strains (Fig. 3A and B). These decreased proinflammatory gene expression signatures are consistent with the effective phagocytosis of the mutants and their overall reduced virulence.

NMD5 is only required for virulence in the presence of fully active immune attack

Given that *nmd5*Δ/Δ infections are associated with greater phagocytosis and thus infection containment, and its role in *C. albicans* has not been previously described, we sought to determine if its primary role in virulence is in immune evasion. In *Saccharomyces cerevisiae, Sc*Nmd5p is required for transport of *Sc*Hog1p and *Sc*Crz1p into the nucleus, and *ScNMD5* mutants are sensitive to salt stress imposed by NaCl, LiCl, $MnCl_2$, and $CaCl_2$ (48–50). We therefore tested if *C. albicans nmd5*Δ/Δ was also sensitive to salt stress, oxidative stress, or pH. While *nmd5*Δ/Δ formed smaller colonies on regular YPD plates, its relative ability to grow on YPD was unchanged with any of these stresses (Fig. S5).

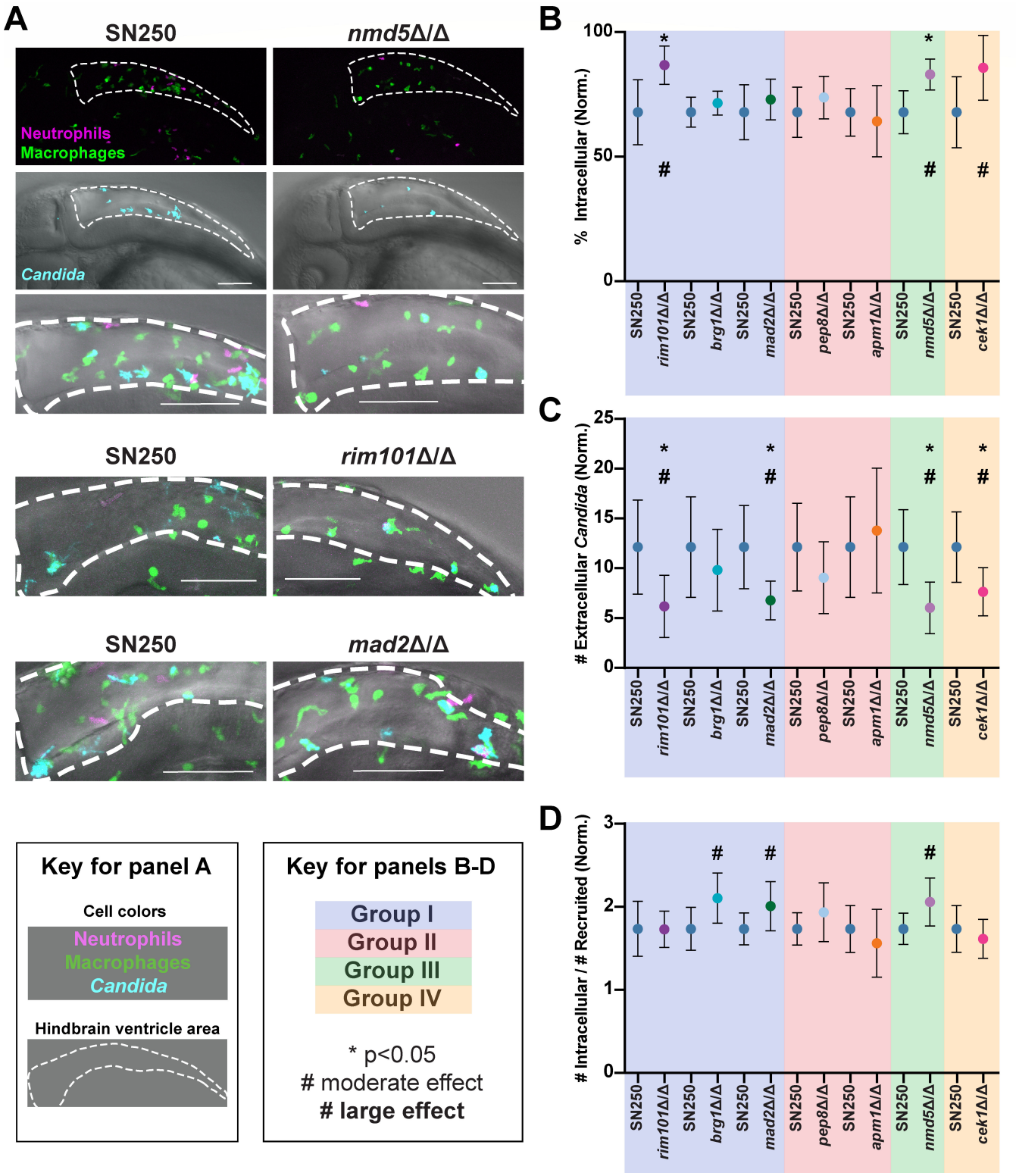

FIG 6 Phagocytosis of hypovirulent *C. albicans* mutants. (A) Example representative images from *nmd5*Δ/Δ, *rim101*Δ/Δ and *mad2*Δ/Δ-infected fish, along with SN250-infected controls, at 4–6 hours postinfection. Images were scored by eye for the number of macrophages (Mpeg1-GFP+ cells) shown in green and the number of neutrophils (LysC-dsRed+ cells) in magenta recruited to the infection, as well as if the *Candida* was intracellular or extracellular. Scale bar is 100 µm. (B–D) Quantification of phagocytosis-related phenotypes. There are separate SN250 columns for each set of experiments, as the mutant was compared to wild type in the same experiments. (B) Plots of the percent intracellular *Candida* normalized to the average percent intracellular *Candida* for SN250. (C) Plots showing

(Continued on next page)

Fig 6 (Continued)

the number of extracellular *Candida* normalized to the average amount for SN250. (D) Plots showing the number of intracellular *Candida*, divided by the number of cells recruited, normalized to the average for SN250. (B–D) Shading indicates Groups I–IV based on similar interaction phenotypes (Fig. 4). Means and 95% confidence intervals are plotted. Statistics were performed from pooled data from at least three independent experiments for each mutant, for approximately 25 fish per strain imaged. Hedges bias-corrected effect sizes and significance were determined for each mutant. * indicates $P < 0.05$, # indicates a moderate effect, while a bold # indicates a strong effect.

We reasoned that if the virulence defect that we observed for *nmd5*Δ/Δ was due to a failure to evade phagocytosis, then limiting the immune response should enhance the virulence of this mutant. We tested this in several ways. First, we treated infected fish with dexamethasone, a general immunosuppressant that regulates macrophage activity in zebrafish (51). As expected based on previous results, *nmd5*Δ/Δ was less virulent than SN250 in the control dimethyl sulfoxide (DMSO)/vehicle treatment condition (Fig. 9A, $P = 0.014$). Dexamethasone immunosuppression increased the virulence of *nmd5*Δ/Δ and eliminated the difference in virulence between *nmd5*Δ/Δ and its wild-type SN250 control (Fig. 9A, $P_{adj} < 0.0006$). We then selectively inactivated NADPH oxidase, knocking down $p47^{phox}$, to reduce phagocyte recruitment to and phagocytosis of *C. albicans* (30). As expected based on previous results, *nmd5*Δ/Δ was less virulent than SN250 in the control STD morpholino condition, and SN250 was more virulent in the $p47^{phox}$ morphant fish as compared to the STD control morphants (Fig. 9B; $P = 0.0002$ and $P = 0.039$, respectively). This gene-directed inactivation caused *nmd5*Δ/Δ to become more virulent ($P_{adj} = 0.0012$) and eliminated any difference in survival between SN250- and *nmd5*Δ/Δ-infected fish (Fig. 9B). Lastly, we performed yolk infections, as there is a delayed/weaker immune response to yolk infection relative to hindbrain infection (52). In yolk infections, we also observed no significant difference in the virulence of *nmd5*Δ/Δ compared to SN250 (Fig. 9C). These three models of reduced immune response/immunosuppression consistently show that *nmd5*Δ/Δ is just as virulent as wild-type SN250 when innate immunity is limited, suggesting that its lack of virulence is due to its failure to evade the immune response.

DISCUSSION

Candida albicans has evolved over many generations with vertebrate hosts and has developed the ability to avoid immune clearance through activities such as filamentous growth, masking of cell wall epitopes, production of a toxin, and avoidance of antibody opsonization (6–14). However, we still know little about how each of these abilities affects immune evasion during vertebrate infection, and we know even less about which fungal genes and pathways regulate immune evasion. The transparency of the larval zebrafish model is a powerful tool that can be utilized to elucidate the different mechanisms of immune evasion in *C. albicans*, especially combined with its cost-effectiveness. Previous work in this infection model has shown that differential immune recruitment and fungal containment through phagocytosis represent important predictors for the fate of individual hosts (29, 30). These favorable aspects of the model

	GROUP I			GROUP II		GROUP III	GROUP IV
Mutant	***rim101* Δ/Δ**	***brg1* Δ/Δ**	***mad2* Δ/Δ**	***pep8* Δ/Δ**	***apm1* Δ/Δ**	***nmd5* Δ/Δ**	***cek1* Δ/Δ**
Morphogenesis *in vivo*	**Down**	**Down**	NO CHANGE	**Down**	**Down**	NO CHANGE	NO CHANGE

Regular text: 0.2<p<0.05	Shaded lightly: Moderate Effect	Green: Decreased relative to WT
Bold: p<0.05	Shaded heavily: Strong Effect	Red: Increased relative to WT

FIG 7 Fungal morphology at 4–6 hpi. Mutant fungal morphology was scored at 4–6 hpi, relative to wild-type fungal morphology in the same experiment. Two of the three Group I mutants and both the Group II mutants had decreased filamentous growth at 4–6 hpi. "Down" text indicates decreased filamentous morphology (pseudohyphal/hyphal). Bold lettering indicates $P < 0.05$. Heavy shading indicates strong effect size; light shading indicates moderate effect size.

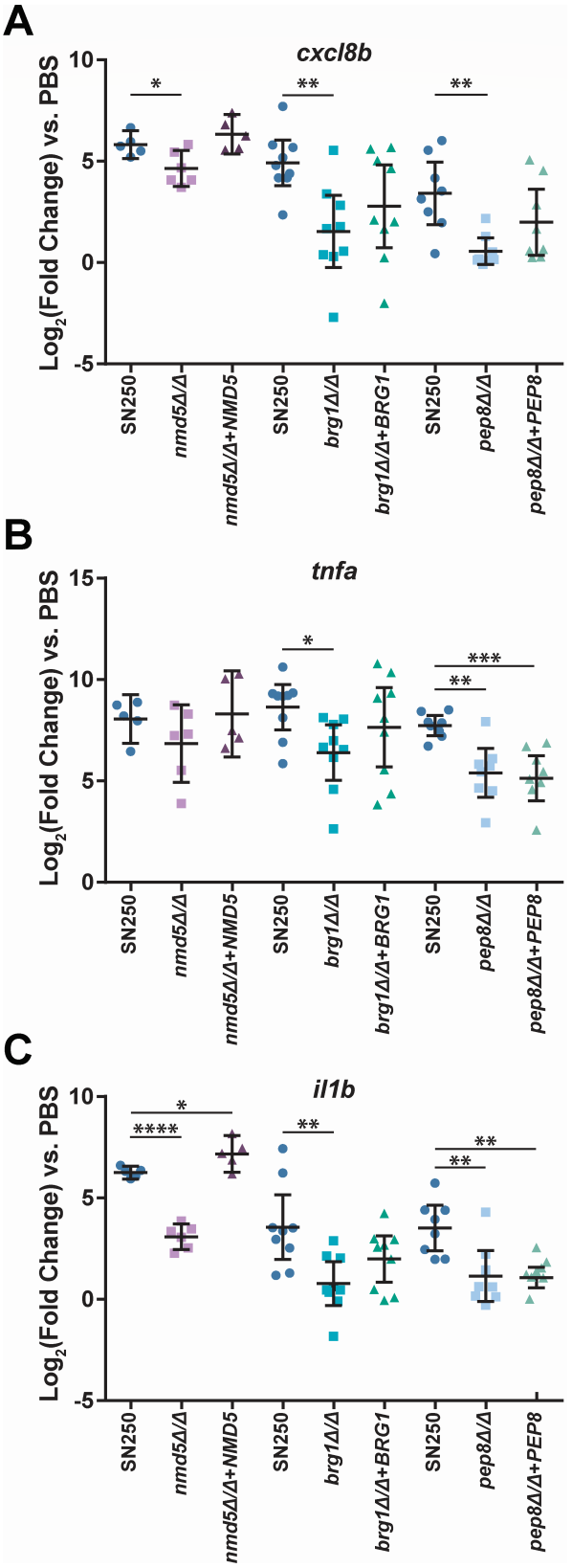

FIG 8 Hypovirulent *C. albicans* mutants elicit a reduced proinflammatory expression at 24 hpi. Expression of *cxcl8b* (A), *tnfa* (B), or *il1b* (C) by qPCR analysis of fish infected with WT (SN250), mutant (*nmd5*Δ/Δ, *brg1*Δ/Δ, or *pep8*Δ/Δ), or complemented (*nmd5*Δ/Δ+NMD5, *brg1*Δ/Δ+BRG1, or *pep8*Δ/Δ+PEP8) *C. albicans*

(Continued on next page)

Fig 8 (Continued)

at 24 hpi. Each point represents a pool of at least five larvae, and data were pooled from three (*NMD5*) or four (*BRG1* and *PEP8*) independent experiments. Gene expression was normalized to *gapdh*, and induction was determined relative to PBS mock-infected larvae. Significance was determined by one-way ANOVA with Dunnett's multiple comparisons tests.

led us to complete the first medium-scale screen of 131 *C. albicans* mutants for virulence, with subsequent analysis for early immune-mediated fungal phagocytosis. This screen characterized several new and known virulence genes as having previously unknown roles in limiting innate immune responses at the infection site. We also identified *NMD5* as a new virulence factor that enables immune evasion.

This is the first single-mutant infection screen of more than 100 individual *C. albicans* mutants in any vertebrate infection model, made possible using a zebrafish model. Very few virulence screens of more than 100 *C. albicans* mutants have been conducted, all using pooled/barcode screening methodology (31, 53, 54). While this is a powerful method, secreted signals and virulence factors that affect the overall environment of the infection site will be missed due to the majority prevalence of cells lacking the phenotype. Pooled virulence screens also score competitive index rather than virulence, *per se*, potentially missing virulence factors. We chose a zebrafish larval hindbrain infection model to screen individual mutants because it overcomes these drawbacks, reproduces many aspects of murine disseminated infection, and provides a useful infection route for quantifying phagocyte recruitment and response (27, 30, 55). As expected, due to the limitations of pooled screening, several mutants that are hypovirulent in both murine tail vein infection and in our screen were missed in the previous pooled screens (*rim101*Δ/Δ, *brg1*Δ/Δ, *cek1*Δ/Δ).

Of the seven mutants identified here, only four mutants—in *RIM101*, *BRG1*, *MAD2*, *CEK1*—have been tested in single-strain murine tail vein infections; all of them are hypovirulent (Table S4) (45, 56–58). Pooled screens have identified mild defects in competitive index for each of these other three mutants (31, 43). All the mutants with intermediate virulence defects in our model that have been tested in mouse tail vein infection are also hypovirulent, suggesting that this class represents a mine of new virulence genes, many of which are uncharacterized with only an ORF number (4). However, the converse is not true, and some mutants hypovirulent in the mouse were not hypovirulent in our study, suggesting that there may be some murine-specific virulence factors. The high concordance between mouse and zebrafish results reinforces the conservation of infection mechanisms in both hosts; this suggests that the three genes still untested for virulence in mice (*APM1*, *PEP8*, and *NMD5*) are most likely of importance in murine (and human) disease.

The zebrafish has the unique advantage of allowing intravital observation of the early innate immune response, which enabled us to group the hypovirulent mutants into four classes. As expected, our screen revealed that increases in phagocytosis efficiency were associated with lower virulence for most of the mutants (Classes I, III, and IV). For some mutant infections, phagocyte numbers were unchanged or decreased, while fungal phagocytosis levels of the mutants matched or exceeded those of wild-type cells (Classes I, II, and III). In these infections, a more robust rapid phagocytosis response may limit later phagocyte recruitment at 4–6 hpi and ultimately result in lower inflammatory gene expression at later time points. Consistent with this idea, highly effective phagocytosis correlates with reduced epithelial NF-kB activation during mucosal *Candida* infection, which is also in line with the lower cytokine production found here at 24 hpi (59).

The cell wall and fungal morphology regulate phagocytosis by macrophages and neutrophils, with β-glucan masking and filamentous shape leading to impaired phagocytosis (9, 43). *BRG1* and *PEP8*, both in the Morphogenesis class, have not previously been identified as regulating immune responses, although both are linked to *Candida* virulence. The mechanisms underlying the roles of these genes in regulating early immune responses are unknown, although their putative functions in vesicle

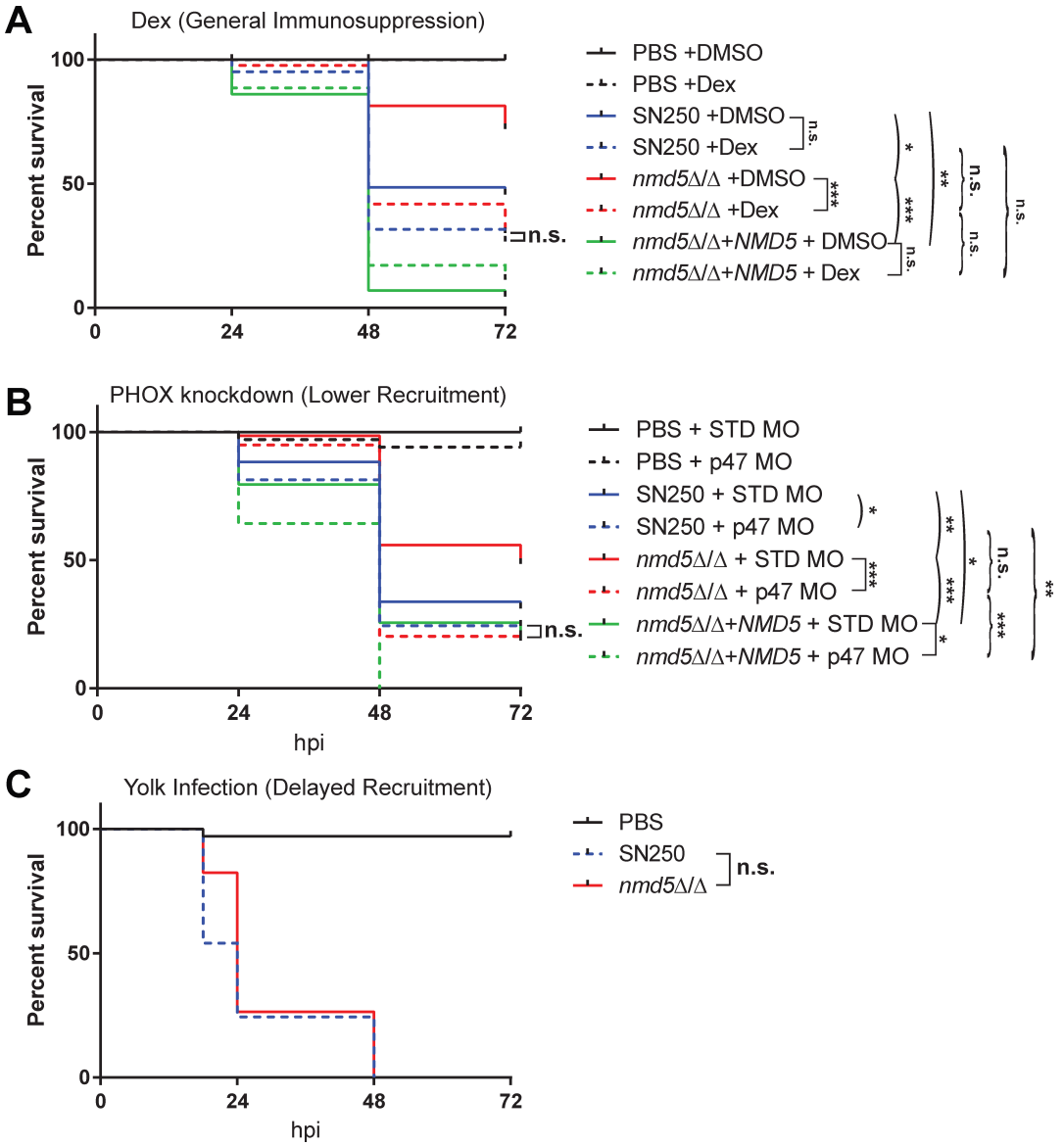

FIG 9 *nmd5*Δ/Δ has fully restored virulence in fish with a reduced immune response. (A) Kaplan-Meier survival curve of dexamethasone-treated hindbrain-injected fish with PBS (*n* = 28), SN250 (*n* = 41), *nmd5*Δ/Δ (*n* = 43), or *nmd5*Δ/Δ+*NMD5* (*n* = 35), or DMSO fish injected with PBS (*n* = 28), SN250 (*n* = 36), *nmd5*Δ/Δ (*n* = 43), or *nmd5*Δ/Δ+*NMD5* (*n* = 43). Data pooled from three independent experiments. (B) Kaplan-Meier survival curve of standard morphant fish injected with PBS (*n* = 22), SN250 (*n* = 46), *nmd5*Δ/Δ (*n* = 39), or *nmd5*Δ/Δ+*NMD5* (*n* = 35), and p47 morphant fish injected with PBS (*n* = 20), SN250 (*n* = 59), *nmd5*Δ/Δ (*n* = 26), or *nmd5*Δ/Δ+*NMD5* (*n* = 34). Data pooled from four independent experiments. (C) Kaplan-Meier survival curve of PBS (*n* = 34), SN250 (*n* = 37), or *nmd5*Δ/Δ (*n* = 34) yolk-injected fish. Data pooled from two independent experiments. Statistics were performed as described in detail in Materials and Methods. Pairwise comparisons that are shown by arcs are confirmatory based on previous experiments; those shown by brackets are exploratory and adjusted for multiple comparisons by Bonferroni correction. Square brackets show if there is an effect of an immune perturbation on survival; curved brackets show if there is an effect of genotype on survival in the context of an immune perturbation. n.s., $P_{adj} > 0.05$; *$P_{adj} < 0.05$; **$P_{adj} < 0.01$; ***$P_{adj} < 0.001$.

transport and biofilm formation both have connections to filamentous growth and surface adhesion proteins that may limit phagocytosis (41, 43, 45, 48, 60). Both mutants produced fewer elongated cells *in vivo*. Because larger filamentous cells are engulfed less efficiently, these minor deficiencies in elongation could lead to earlier fungal phagocytosis (43). These and other mutants may also have alterations in their cell walls that eliminate structural mechanisms for phagocytic evasion, although the only strains with known cell wall defects are *cek1*Δ/Δ, which has more β-glucan exposure and recruits more phagocytes to the infection site, and *rim101*Δ/Δ, which regulates cell wall genes

(9, 61, 62). This conservation of phenotypes again suggests that the zebrafish is a good model for examining the effect of altered cell wall on early phagocytosis and immune recruitment—even if zebrafish do not have a direct sequence homolog of the key pattern recognition receptor for exposed β-glucan, Dectin-1 (63).

The most pronounced increase in early phagocytic efficiency occurred in infections of fungi lacking *NMD5*, a mutant in the Infectivity class, which is predicted to regulate nuclear protein import and ionic stresses, based on work in baker's yeast (48, 49). The *C. albicans nmd5*Δ/Δ mutant has defects in white-opaque switching, and its expression is altered in phagocyte interaction, biofilm growth, and osmotic stress (64–70). Its differential expression upon neutrophil and macrophage challenges is consistent with its role in limiting phagocytosis (66, 67, 69, 70). In contrast to its function in baker's yeast, the *C. albicans nmd5*Δ/Δ mutant is not hypersensitive to stress conditions, suggesting a significant divergence in gene function between the species—as has been observed previously (71, 72). Instead, the function of *CaNMD5* is clearly related to immune evasion—the mutant loses its virulence disadvantage when the innate immune response is compromised by any of three methods. Given the likely role of Nmd5p in nuclear import of transcription factors, it will be interesting to identify differential transcription patterns in this mutant that may account for the loss in immune evasion.

Overall, our findings reinforce the relevance of studying *Candida*-innate immune events in zebrafish by intravital imaging, identify several new hypovirulent mutants, describe early immune evasion-related phenotypes for all of the mutants, and characterize *NMD5* as a new and important virulence factor required to limit innate immune phagocytosis. These results highlight the importance of an effective early innate immune response that engulfs *C. albicans* cells rapidly to limit germination during infection. We expect that future intravital timelapse experiments in the zebrafish at high spatio-temporal resolution will further characterize how phagocytes interact with these mutants and thereby shed light on conserved mechanisms that regulate early events in candidiasis in vertebrate hosts.

MATERIALS AND METHODS

C. albicans strains and growth conditions

C. albicans mutant strains for screening were obtained from the Noble library (31) (Table 1). For infection, strains were grown on yeast-peptone-dextrose (YPD) agar at 30°C (20 g/L glucose, 20 g/L peptone, 10 g/L yeast extract, 20 g/L agar; Difco, Livonia, MI, USA). Single colonies were picked from plates, inoculated into 5 mL liquid YPD, and grown overnight on a wheel at 30°C. Overnight cultures were resuspended in phosphate-buffered saline (PBS, 5 mM sodium chloride, 0.174 mM potassium chloride, 0.33 mM calcium chloride, 0.332 mM magnesium sulfate, 2 mM HEPES in Nanopure water, pH = 7) and stained with Calcofluor white (750 µg/mL) when necessary. Cultures were washed twice with PBS, and the concentration was adjusted to 1×10^7 CFU/mL in PBS for injection. For imaging, strains were transformed with pENO1-iRFP-NAT^r according to reference 42. Strains were screened by fluorescence microscopy and flow cytometry to pick the brightest isolates, and the integration site at the *ENO1* locus was confirmed by PCR as described (42). Full deletion of *RBT1* from SN250 was achieved using the SAT-flipper method as described previously (73) using LiAC transformation. The deletion cassette was generated by integrating 514 bp up and 485 bp downstream of *RBT1* into a pSFS2 derivative (73) and was excised by restriction digest with KpnI and SacI.

Complementation of mutant strains

Complementation constructs were ordered from GenScript (Piscataway, NJ, USA) in the pUC57 backbone and contain the ORF with 200 bp upstream and 50 bp downstream, followed by *Candida dubliniensis ARG4* (Fig. S6A). Restriction sites were eliminated from the ORF during gene synthesis. A restriction site was designed within the 200 bp

TABLE 1 *Candida albicans* strains

Strain	Parental strain	Genotype	Reference
*yfg*Δ/Δ[a]	SN152	*ura3*Δ-*iro1*Δ::*imm*^{434}/*URA3-IRO1 his1*Δ/*his1*Δ *arg4*Δ/*arg4*Δ *leu2*Δ/*leu2*Δ *yfg*Δ::*C.mLEU2/yfg*Δ::*C.dHIS1 YFG::C.d.ARG4*	(31)
SN250-iRFP	SN152	*ura3*Δ-*iro1*Δ::*imm*^{434}/*URA3-IRO1 his1*Δ/*his1*Δ *arg4*Δ/*arg4*Δ *leu2*Δ::*C.m.LEU2/leu2*Δ::*C.d.HIS1 pENO1-iRFP-NATR*	(31), this study
*rbt1*Δ/Δ$^{968\text{-}2166}$-iRFP	SN152	*ura3*Δ-*iro1*Δ::*imm*^{434}/*URA3-IRO1 his1*Δ/*his1*Δ *arg4*Δ/*arg4*Δ *leu2*Δ/*leu2*Δ *rbt1*Δ$^{967\text{-}2166}$::*C.mLEU2/ rbt1*Δ$^{967\text{-}3166}$::*C.dHIS1 pENO1-iRFP-NATR*	(31), this study
*cht2*Δ/Δ-iRFP	SN152	*ura3*Δ-*iro1*Δ::*imm*^{434}/*URA3-IRO1 his1*Δ/*his1*Δ *arg4*Δ/*arg4*Δ *leu2*Δ/*leu2*Δ *cht2::C.mLEU2/cht2::C.dHIS1 pENO1-iRFP-NATR*	(31), this study
*rim101*Δ/Δ-iRFP	SN152	*ura3*Δ-*iro1*Δ::*imm*^{434}/*URA3-IRO1 his1*Δ/*his1*Δ *arg4*Δ/*arg4*Δ *leu2*Δ/*leu2*Δ *rim101::C.mLEU2/rim101::C.dHIS1 pENO1-iRFP-NATR*	(31), this study
*brg1*Δ/Δ-iRFP	SN152	*ura3*Δ-*iro1*Δ::*imm*^{434}/*URA3-IRO1 his1*Δ/*his1*Δ *arg4*Δ/*arg4*Δ *leu2*Δ/*leu2*Δ *brg1::C.mLEU2/brg1::C.dHIS1 pENO1-iRFP-NATR*	(31), this study
*cek1*Δ/Δ-iRFP	SN152	*ura3*Δ-*iro1*Δ::*imm*^{434}/*URA3-IRO1 his1*Δ/*his1*Δ *arg4*Δ/*arg4*Δ *leu2*Δ/*leu2*Δ *cek1::C.mLEU2/cek1::C.dHIS1 pENO1-iRFP-NATR*	(31), this study
*pep8*Δ/Δ-iRFP	SN152	*ura3*Δ-*iro1*Δ::*imm*^{434}/*URA3-IRO1 his1*Δ/*his1*Δ *arg4*Δ/*arg4*Δ *leu2*Δ/*leu2*Δ *pep8::C.mLEU2/pep8::C.dHIS1 pENO1-iRFP-NATR*	(31), this study
*nmd5*Δ/Δ-iRFP	SN152	*ura3*Δ-*iro1*Δ::*imm*^{434}/*URA3-IRO1 his1*Δ/*his1*Δ *arg4*Δ/*arg4*Δ *leu2*Δ/*leu2*Δ *nmd5::C.mLEU2/nmd5::C.dHIS1 pENO1-iRFP-NATR*	(31), this study
*apm1*Δ/Δ-iRFP	SN152	*ura3*Δ-*iro1*Δ::*imm*^{434}/*URA3-IRO1 his1*Δ/*his1*Δ *arg4*Δ/*arg4*Δ *leu2*Δ/*leu2*Δ *apm1::C.mLEU2/apm1::C.dHIS1 pENO1-iRFP-NATR*	(31), this study
*mad2*Δ/Δ-iRFP	SN152	*ura3*Δ-*iro1*Δ::*imm*^{434}/*URA3-IRO1 his1*Δ/*his1*Δ *arg4*Δ/*arg4*Δ *leu2*Δ/*leu2*Δ *mad2::C.mLEU2/mad2::C.dHIS1 pENO1-iRFP-NATR*	(31), this study
*ece1*Δ/Δ - dtom	BWP17	*ura3::imm434/ura3::imm434 iro1::imm434/iron1::imm434 his1::hisG/his1::hisG arg4::hisG/arg4::hisG ece1::HIS2/ece1::ARG4 RPS1/rps1::URA3 ENO1/eno1::dTom-NATR*	(74)
*ece1*Δ/Δ+*ECE1* - dtom	BWP17	*ura3::imm434/ura3::imm434 iro1::imm434/iron1::imm434 his1::hisG/his1::hisG arg4::hisG/arg4::hisG ece1::HIS2/ece1::ARG4 RPS1/rps1::URA3-ECE1 ENO1/eno1::dTom-NATR*	(74)
NRG1^{OEX}-iRFP	THE21	*ade2::hisG:/ade2::hisG ura3::imm434/ura3::imm434::URA2- tetO ENO1/eno1::ENO1 tetR – ScHAP4AD-3XHA-ADE2 pENO1-iRFP-NATR*	(75, 76)
*rbt1*Δ/Δ$^{968\text{-}2166}$+*RBT1*	*rbt1*Δ/Δ$^{968\text{-}2166}$	*ura3*Δ-*iro1*Δ::*imm*^{434}/*URA3-IRO1 his1*Δ/*his1*Δ *arg4*Δ/*arg4*Δ *leu2*Δ/*leu2*Δ *rbt1*Δ$^{967\text{-}2166}$::*C.mLEU2/ rbt1*Δ$^{967\text{-}2166}$::*C.dHIS1 RBT1::C.d.ARG4*	This study
*rim101*Δ/Δ+*RIM101*	*rim101*Δ/Δ	*ura3*Δ-*iro1*Δ::*imm*^{434}/*URA3-IRO1 his1*Δ/*his1*Δ *arg4*Δ/*arg4*Δ *leu2*Δ/*leu2*Δ *rim101*Δ::*C.mLEU2/rim101*Δ::*C.dHIS1 RIM101::C.d.ARG4*	This study
*brg1*Δ/Δ+*BRG1*	*brg1*Δ/Δ	*ura3*Δ-*iro1*Δ::*imm*^{434}/*URA3-IRO1 his1*Δ/*his1*Δ *arg4*Δ/*arg4*Δ *leu2*Δ/*leu2*Δ *brg1*Δ::*C.mLEU2/brg11*Δ::*C.dHIS1 BRG11::C.d.ARG4*	This study
*cek1*Δ/Δ+*CEK1*	*cek1*Δ/Δ	*ura3*Δ-*iro1*Δ::*imm*^{434}/*URA3-IRO1 his1*Δ/*his1*Δ *arg4*Δ/*arg4*Δ *leu2*Δ/*leu2*Δ *cek1*Δ::*C.mLEU2/cek1*Δ::*C.dHIS1 CEK1::C.d.ARG4*	This study
*pep8*Δ/Δ+*PEP8*	*pep8*Δ/Δ	*ura3*Δ-*iro1*Δ::*imm*^{434}/*URA3-IRO1 his1*Δ/*his1*Δ *arg4*Δ/*arg4*Δ *leu2*Δ/*leu2*Δ *pep8*Δ::*C.mLEU2/pep8*Δ::*C.dHIS1 PEP8::C.d.ARG4*	This study
*nmd5*Δ/Δ+*NMD5-mNeon -iRFP*	*nmd5*Δ/Δ-*iRFP*	*ura3*Δ-*iro1*Δ::*imm*^{434}/*URA3-IRO1 his1*Δ/*his1*Δ *arg4*Δ/*arg4*Δ *leu2*Δ/*leu2*Δ *ndm5*Δ::*C.mLEU2/nmd5::C.dHIS1 NMD5-mNeon::C.d.ARG4 pENO1-iRFP-NATR*	This study
*amp1*Δ/Δ+*APM1*	*apm1*Δ/Δ	*ura3*Δ-*iro1*Δ::*imm*^{434}/*URA3-IRO1 his1*Δ/*his1*Δ *arg4*Δ/*arg4*Δ *leu2*Δ/*leu2*Δ *apm21*Δ::*C.mLEU2/apm1*Δ::*C.dHIS1 APM1::C.d.ARG4*	This study
*mad2*Δ/Δ+*MAD2*	*mad2*Δ/Δ	*ura3*Δ-*iro1*Δ::*imm*^{434}/*URA3-IRO1 his1*Δ/*his1*Δ *arg4*Δ/*arg4*Δ *leu2*Δ/*leu2*Δ *mad2*Δ::*C.mLEU2/mad2*Δ::*C.dHIS1 MAD2::C.d.ARG4*	This study
*rbt1*Δ/Δ	SN250	*ura3*Δ-*iro1*Δ::*imm*^{434}/*URA3-IRO1 his1*Δ/*his1*Δ *arg4*Δ/*arg4*Δ *leu2*Δ::*C.m.LEU2/leu2*Δ::*C.d.HIS1 rbt1*Δ$^{1\text{-}2166}$/Δ$^{1\text{-}2166}$	This study

[a]*yfg*, your favorite gene. See Table S1 for a complete list of mutant strains.

upstream region, an NdeI cutsite at the start of the ORF, a BamHI restriction site in the *ARG4* upstream region, and a BglII site in the downstream *ARG4* region. An *NMD5* complementation construct was ordered from Twist Bioscience (South San Francisco, CA, USA) without *ARG4*. This construct included an upstream XbaI restriction site, a 200 bp *NMD5* upstream region containing an XhoI restriction site, the *NMD5* ORF, the mNeon ORF (77) flanked by NcoI restriction sites and a PacI restriction site, then 50 bp of the *NMD5* downstream region, and a BamHI site in an *ARG4* upstream region. This region

was then cloned into the GenScript pUC57 backbone by cutting with the XbaI and BamHI to remove the *PEP8* region and replace it with the *NMD5* region to get an *NMD5* construct containing *ARG4* (Fig. S6B). For complementation, constructs were cut with the appropriate restriction enzymes, and a LiAC transformation was performed using rescue of the *ARG4* autotrophy as a selection marker. PCR was performed to ensure correct integration. *NMD5* complementation colonies were screened by flow cytometry for mNeon-positive cells. Sequences of the complementation constructs are provided in Table S5. To check for functional complementation of mutants that have known morphogenesis defect (Fig. S1), we assessed the growth on Spider media (for *BRG1*, *CEK1*, and *PEP8* strains) or in M199 at pH 4 and pH 8 (for *RIM101* strains). Briefly, to test the growth on Spider media, we grew SN250, mutant, and complemented strains overnight at 30°C in 5 mL YPD. Overnight cultures were diluted in PBS, and 100 µL of 1×10^2 cells/mL was spread onto Spider plates. Plates were incubated at 30°C and imaged after 7 and 14 days of growth. For *RIM101* strains SN250, *rim101*Δ/Δ, and complemented strains were grown overnight at 30°C in 5 mL YPD. Fifty microliters of overnight culture was inoculated into M199 pH 4 and pH 8 and grown at 37°C for 4 hours. Strains were then imaged on a Zeiss Axio Observer Z1 microscope (Carl Zeiss Microimaging, Thornwood, NJ, USA) to assess filamentous growth.

Growth of *nmd5*Δ/Δ on different media to assess salt tolerance

Overnight cultures were grown at 30°C in 5 mL YPD. Cells (3×10^7) from the overnight culture were inoculated into 5 mL fresh YPD and incubated on a roller drum for 4 hours. After 4 hours, 10-fold serial dilutions were performed out to 10^{-5} in PBS, and 3 µL of the 10^0 to 10^{-5} dilutions was spotted onto plates. Plates include YPD, M199 pH 8, M199 pH 4, YPD + 400 mM NaCl, YPD + 1.5 mM H_2O_2, YPD + 400 mM $CaCl_2$, YPD + 150 mM LiCl, and YPD + 6 mM $MnCl_2$. Plates were incubated at 30°C for 48 hours and imaged after 24 and 48 hours of incubation. Strains were spotted in duplicate on two plates, and three replicates were performed.

Zebrafish care and maintenance

Adult zebrafish were held in the University of Maine Zebrafish facility at 28°C in a recirculating system (Aquatic Habitats, Apopka, FL, USA) under a 14 hour/10 hour light/dark cycle and fed Hikari micropellets (catalogue number HK40; Pentair Aquatic Ecosystems) (Table 2).

Zebrafish infections

Zebrafish were raised at 33°C for the first 24 hours, in E3 plus 0.3 mg/L methylene blue for the first 6 hours then in E3 plus 1-phenyl-2-thio urea (PTU) (0.02 mg/mL, Sigma-Aldrich, St. Louis, MO, USA) thereafter. At 24 hours post-fertilization (hpf), embryos were dechorionated. Injection solutions were made up at 1×10^7 cells/mL in PBS and stained with Calcofluor white (750 µg/mL) as necessary to visualize non-fluorescent or far-red candida by eye. Embryos were anesthetized in tricaine (160 µg/mL; Tricaine; Western Chemicals, Inc., Ferndale, WA, USA) at the prim-25 stage for both hindbrain and yolk infection (55). Embryos that were injured during the injection process were removed. After infection, fish were placed at 30°C for the remainder of the experiment and monitored for survival out to 72 hpi. Fish were screened after injection on a Zeiss Axio Observer Z1 microscope (Carl Zeiss Microimaging, Thornwood, NJ, USA) to ensure that they received between 10 and 25 *C. albicans* cells.

Large-scale virulence screening

For large-scale virulence screening, five *C. albicans* mutants were tested along with SN250 WT control and PBS mock-infected fish in one experiment with approximately 50 fish per strain. Due to the large number of injected fish, fish were not screened

after injection, and *C. albicans* was not stained with Calcofluor white. As another check, if survival of SN250-infected fish fell outside of 5.3%–72.18% survival (by 72 hpi), the experiment was eliminated from consideration, and all mutant strains were retested.

Dexamethasone treatment

For dexamethasone experiments, dexamethasone (Millipore Sigma, Calbiochem, 10 mg/mL stock) or DMSO (vehicle control) was added to the E3+PTU 1 hour before infection and maintained throughout the experiment. A final concentration of 50 µg/mL dexamethasone, 0.5% DMSO was used. Injections in the hindbrain ventricle were otherwise performed as described above.

Morpholino injection

Embryos were injected between the 1- and 4-cell stage with standard (1 ng/nL, CCT CTTACCTCAGTTACAATTTATA) or p47^{phox} (2.5 ng/nL, CGGCGAGATGAAGTGTGTGAGCGAG) morpholinos. Morpholino injection solutions were prepared in 0.3 × Danieau buffer [17.4 mM NaCl, 0.21 mM KCl, 0.12 mM $MgSO_4$•$7H_2O$, 0.18 mM $Ca(NO_3)_2$, 1.5 mM Hepes, pH 7.2] with 0.16% fluorescent dextran and 0.001% phenol red. Morpholino-injected fish were kept in plain E3 until 12 hpf, when methylene blue and PTU (0.02 mg/mL) were added. At the time of infection, fish were switched to E3+PTU and maintained in E3+PTU throughout infection. Fish were screened for dextran incorporation and discarded from the experiment if they did not show fluorescence throughout the fish. Hindbrain infections in morphant fish were performed at the prim-25 stage as described above.

Quantitative real-time PCR

Fish were infected as described above, screened for correct inoculum (10–25 fungal cells), and euthanized at 4 hpi or 24 hpi for qPCR. Pools of 5–10 larvae were homogenized in TRIzol (Invitrogen, Carlsbad, CA, USA) and stored at −80°C. RNA isolation was performed using the Direct-zol RNA Miniprep kit (Zymo Research, Irvine, CA, USA) following their protocol. cDNA was synthesized from 500 ng of RNA using iSCRIPT reverse transcription (RT) supermix for RT-qPCR (Bio-Rad, Hercules, CA, USA). qPCR was performed using SsoAdvanced Universal SYBR Green Supermix (Bio-Rad) with 1 µL of cDNA in 10 µL reactions with primers listed in Table 3. qPCR was run on a CFX96 Real time system, C1000 touch thermal cycler (Bio-Rad).

Fluorescence microscopy

For analysis of the phagocyte response at 4–6 hpi, embryos were placed in 0.4% low melting point agarose in E3 with 160 µg/mL tricaine in a glass bottom 24-well plate (MatTek Corporation, Ashland, MA, USA), and the hindbrain ventricle was imaged. Images were taken on an Olympus IX-81 inverted microscope with an FV-1000 laser scanning confocal system (Olympus, Waltham, MA, USA) with a 20× (0.75 NA) objective with 5 µm increments for approximately 25–35 slices.

Image analysis

Images were imported into Fiji (ImageJ) and made into composite four-channel z-stacks for quantification. The number of *mpeg1*:GFP+ or *lysC*:dsRed+ cells was counted

TABLE 2 Zebrafish lines

Zebrafish line	Allele	Source/reference
AB (wild type)	n/a[a]	Zebrafish International Resource Center
Tg(mpeg1:EGFP)/Tg(lysC:dsRed)	gl22Tg nz50Tg	(78, 79)

[a]n/a, not applicable.

manually for the hindbrain region throughout the z-stack. In addition, *C. albicans* cells were manually counted for whether they were intracellular (inside *mpeg1*:GFP+, *lysC*:dsRed+, or other) or extracellular to determine the percent of *C. albicans* cells that were taken up by the host. The total number of cells recruited to the infection included *mpeg1*:GFP+ cells, *lysC*:dsRed+ cells, as well as non-fluorescent cells phagocytosing *Candida*. Fish were excluded from the total cells recruited count if they did not contain both GFP+ and dsRed+ cells.

Statistical analysis

Statistical analysis was performed using GraphPad Prism software. To calculate the z-score for quantifying screening results, we measured the mean and standard deviation of 72 hpi percent survival for all of the SN250 (control) infections and then calculated ([Survival % Mutant] – [Mean Survival % Control]) / Standard Deviation of Survival % Control. For analysis of survival in non-screen experiments, Kaplan-Meier curves were generated from at least three pooled experiments with the same mutant *C. albicans* strains, with SN250 always included in the same experiments, and Mantel-Cox log-rank tests were performed. We utilized Bonferroni corrections to reduce the family-wide error rate in exploratory experiments while omitting this for any hypotheses that were firmly established *a priori* based on data prior to these experiments (83). Non-exploratory hypotheses based on data shown in Fig. 3 were the following: SN250 is more virulent than *nmd5Δ/Δ* but less virulent than *nmd5Δ/Δ+NMD5*, while *nmd5Δ/Δ* is less virulent than both the other strains. Furthermore, we have shown in previous work that p47 morpholino knockdown makes zebrafish more susceptible to wild-type *C. albicans*, so this is confirmatory rather than exploratory (30). Thus, in Fig. 9, the pairwise comparisons shown by arcs (e.g., SN250 vs *nmd5Δ/Δ*) were not Bonferroni corrected for multiple comparisons because the effects of genotype alone were already tested in Fig. 3, and the effect of the p47 MO was already demonstrated (30). For analysis of differences in phagocyte recruitment and phagocytosis, a normality test was performed. If the distribution was not normal, the data were trimmed for outliers (top and bottom 10%), and this allowed for parametric testing. All mutants were compared to wild-type SN250 in each experiment. For simplicity in presenting all data in one graph, data were normalized to WT, SN250 values. For normalization, the average SN250 value for a set of experiments was divided by the average SN250 value for all experiments to get an adjustment value. The value for each individual fish was then divided by this adjustment value to get a normalized value for each fish. Normalized values were used to generate plots, which show the mean and 95% confidence interval. Effect size was determined as described by reference (38) using the effect size calculator (https://f.hubspotusercontent30.net/hubfs/5191137/attachments/ebe/EffectSizeCalculator.xls). A size of greater than 0 and less than 0.3 was qualified as small, greater than 0.3 and less than 0.5 as moderate, and greater than 0.5 as strong (38). Briefly, this is calculated as $(M_1 - M_2)/s_{pooled}$, where $M_1 - M_2$ is the difference between the means, and s_{pooled} is the root mean squared of the two standard deviations. Hedges' factor is used to correct for bias in effect size (84).

ACKNOWLEDGMENTS

We thank Prof. Suzanne Noble for making the mutant library available through the Fungal Genetics Stock Center and Mark Nilan for providing wonderful fish care.

This work is supported by grants from the University of Maine Institute of Medicine (to B.A.B.), Maine INBRE (Honors Pre-thesis and Thesis Fellowships through NIH P20GM103423 to E.B., M.M., and L.S.), and R15AI169393 (to R.T.W.). R.T.W. is a Burroughs Welcome Fund Investigator in the Pathogenesis of Infectious Disease.

AUTHOR AFFILIATIONS

[1]Department of Molecular & Biomedical Sciences, University of Maine, Orono, Maine, USA

TABLE 3 qPCR primers

Gene	Sequence	Reference
cxcl8b	Fw: GCTGGATCACACTGCAGAAA	(80)
	Rv: TGCTGCAAACTTTTCCTTGA	
tnfa	Fw: TTCACGCTCCATAAGACCCA	(81)
	Rv: CCGTAGGATTCAGAAAAGCG	
il1b	Fw: GTCACACTGAGAGCCGGAAG	(59)
	Rv: TGGAGATTCCCAAACACACA	
gapdh	Fw: TGGGCCCATGAAAGGAAT	(82)
	Rv: ACCAGCGTCAAAGATGGATG	

[2]Graduate School of Biomedical Sciences and Engineering, University of Maine, Orono, Maine, USA
[3]Department of Microbiology and Molecular Genetics, McGovern Medical School, The University of Texas Health Science Center at Houston, Houston, Texas, USA

AUTHOR ORCIDs

Pedro Miramon http://orcid.org/0000-0002-6867-7697
Michael C. Lorenz http://orcid.org/0000-0002-7881-8027
Robert T. Wheeler http://orcid.org/0000-0003-3223-7021

FUNDING

Funder	Grant(s)	Author(s)
National Institute of Allergy and Infectious Diseases	1R15AI169393	Bailey A. Blair Emma Bragdon Gursimran Dhillon Nnamdi Baker Lena Stasiak Mya Muthig Robert T. Wheeler
Burroughs Wellcome Fund	PATH	Robert T. Wheeler
National Institute of Allergy and Infectious Diseases	R01AI143304	Pedro Miramon Michael C. Lorenz
National Institute of General Medical Sciences	P20GM103423	Emma Bragdon Lena Stasiak Mya Muthig

AUTHOR CONTRIBUTIONS

Bailey A. Blair, Conceptualization, Data curation, Formal analysis, Investigation, Supervision, Writing – original draft, Writing – review and editing | Emma Bragdon, Investigation, Writing – review and editing | Gursimran Dhillon, Investigation, Writing – review and editing | Nnamdi Baker, Investigation, Supervision, Writing – review and editing | Lena Stasiak, Investigation, Methodology, Writing – review and editing | Mya Muthig, Investigation, Methodology, Writing – review and editing | Pedro Miramon, Investigation, Methodology, Writing – review and editing | Michael C. Lorenz, Supervision, Writing – review and editing | Robert T. Wheeler, Conceptualization, Funding acquisition, Project administration, Supervision, Writing – review and editing

ETHICS APPROVAL

All zebrafish studies were carried out in accordance with the recommendations in the Guide for the Care and Use of Laboratory Animals of the National Research Council (85). All animals were treated in a humane manner and euthanized with Tricaine overdose according to the guidelines of the University of Maine Institutional Animal Care and Use Committee (IACUC) as detailed in protocols A2015-11-03, A2018-10-01, and A2021-09-01.

ADDITIONAL FILES

The following material is available online.

Supplemental Material

Supplemental Tables (mBio00529-25-s0001.xlsx). Tables S1 to S5.
Fig. S1 (mBio00529-25-s0002.tif). Complementation partially restores *in vitro* phenotypes of *brg1*Δ/Δ, *pep8*Δ/Δ, *cek1*Δ/Δ, and *rim101*Δ/Δ mutants.
Fig. S2 (mBio00529-25-s0003.tif). Complementation did not restore the virulence of *cht2*Δ/Δ, *orf19.5547*Δ/Δ, or $rbt^{1968\text{-}2166}$Δ/Δ.
Fig. S3 (mBio00529-25-s0004.tif). Some mutants show fewer elongated cells in the zebrafish hindbrain at 4-6 hours post infection.
Fig. S4 (mBio00529-25-s0005.tif). Expression of inflammatory genes early during *C. albicans* infection.
Fig. S5 (mBio00529-25-s0006.tif). *nmd5*Δ/Δ is not more susceptible to cell stressors.
Fig. S6 (mBio00529-25-s0007.tif). Complementation constructs.
Supplemental Legends and Captions (mBio00529-25-s0008.docx). Legends for Fig. S1–S6 and captions for Tables S1–S5.

REFERENCES

1. Benedict K, Jackson BR, Chiller T, Beer KD. 2019. Estimation of direct healthcare costs of fungal diseases in the United States. Clin Infect Dis 68:1791–1797. https://doi.org/10.1093/cid/ciy776
2. Tsay S, Williams S, Mu Y, Epson E, Johnston H, Farley MM, Harrison LH, Vonbank B, Shrum S, Dumyati G, Zhang A, Schaffner W, Magill S, Vallabhaneni S. 2018. 363. National burden of candidemia, United States, 2017. Open Forum Infect Dis 5:S142–S143. https://doi.org/10.1093/ofid/ofy210.374
3. Ardizzoni A, Wheeler RT, Pericolini E. 2021. It takes two to Tango: how a dysregulation of the innate immunity, coupled with *Candida* virulence, triggers VVC onset. Front Microbiol 12:692491. https://doi.org/10.3389/fmicb.2021.692491
4. Brown GD, Denning DW, Gow NAR, Levitz SM, Netea MG, White TC. 2012. Hidden killers: human fungal infections. Sci Transl Med 4:165rv13. https://doi.org/10.1126/scitranslmed.3004404
5. Smith DJ, Gold JAW, Benedict K, Wu K, Lyman M, Jordan A, Medina N, Lockhart SR, Sexton DJ, Chow NA, Jackson BR, Litvintseva AP, Toda M, Chiller T. 2023. Public health research priorities for fungal diseases: a multidisciplinary approach to save lives. J Fungi (Basel) 9:820. https://doi.org/10.3390/jof9080820
6. Brown R, Priest E, Naglik JR, Richardson JP. 2021. Fungal toxins and host immune responses. Front Microbiol 12:643639. https://doi.org/10.3389/fmicb.2021.643639
7. Goyal S, Castrillón-Betancur JC, Klaile E, Slevogt H. 2018. The interaction of human pathogenic fungi with C-type lectin receptors. Front Immunol 9:1261. https://doi.org/10.3389/fimmu.2018.01261
8. Hernández-Chávez MJ, Pérez-García LA, Niño-Vega GA, Mora-Montes HM. 2017. Fungal strategies to evade the host immune recognition. J Fungi (Basel) 3:51. https://doi.org/10.3390/jof3040051
9. Hopke A, Brown AJP, Hall RA, Wheeler RT. 2018. Dynamic fungal cell wall architecture in stress adaptation and immune evasion. Trends Microbiol 26:284–295. https://doi.org/10.1016/j.tim.2018.01.007
10. Kadosh D. 2019. Regulatory mechanisms controlling morphology and pathogenesis in *Candida albicans*. Curr Opin Microbiol 52:27–34. https://doi.org/10.1016/j.mib.2019.04.005
11. Oliver JC, Ferreira CBRJ, Silva NC, Dias ALT. 2019. *Candida* spp. and phagocytosis: multiple evasion mechanisms. Antonie Van Leeuwenhoek 112:1409–1423. https://doi.org/10.1007/s10482-019-01271-x
12. Ost KS, O'Meara TR, Stephens WZ, Chiaro T, Zhou H, Penman J, Bell R, Catanzaro JR, Song D, Singh S, Call DH, Hwang-Wong E, Hanson KE, Valentine JF, Christensen KA, O'Connell RM, Cormack B, Ibrahim AS, Palm NW, Noble SM, Round JL. 2021. Adaptive immunity induces mutualism between commensal eukaryotes. Nature 596:114–118. https://doi.org/10.1038/s41586-021-03722-w
13. Seider K, Heyken A, Lüttich A, Miramón P, Hube B. 2010. Interaction of pathogenic yeasts with phagocytes: survival, persistence and escape. Curr Opin Microbiol 13:392–400. https://doi.org/10.1016/j.mib.2010.05.001
14. Singh DK, Tóth R, Gácser A. 2020. Mechanisms of pathogenic *Candida* species to evade the host complement attack. Front Cell Infect Microbiol 10:94. https://doi.org/10.3389/fcimb.2020.00094
15. Brown GD. 2011. Innate antifungal immunity: the key role of phagocytes. Annu Rev Immunol 29:1–21. https://doi.org/10.1146/annurev-immunol-030409-101229
16. Dambuza IM, Levitz SM, Netea MG, Brown GD. 2017. Fungal recognition and host defense mechanisms. Microbiol Spectr 5. https://doi.org/10.1128/microbiolspec.funk-0050-2016
17. Jawale CV, Biswas PS. 2021. Local antifungal immunity in the kidney in disseminated candidiasis. Curr Opin Microbiol 62:1–7. https://doi.org/10.1016/j.mib.2021.04.005
18. Lionakis MS, Iliev ID, Hohl TM. 2017. Immunity against fungi. JCI Insight 2:e93156. https://doi.org/10.1172/jci.insight.93156
19. Netea MG, Joosten LAB, van der Meer JWM, Kullberg B-J, van de Veerdonk FL. 2015. Immune defence against *Candida* fungal infections. Nat Rev Immunol 15:630–642. https://doi.org/10.1038/nri3897
20. Drummond RA, Collar AL, Swamydas M, Rodriguez CA, Lim JK, Mendez LM, Fink DL, Hsu AP, Zhai B, Karauzum H, et al. 2015. CARD9-dependent neutrophil recruitment protects against fungal invasion of the central nervous system. PLoS Pathog 11:e1005293. https://doi.org/10.1371/journal.ppat.1005293

21. Drummond RA. 2023. What fungal CNS infections can teach us about neuroimmunology and CNS-specific immunity. Semin Immunol 67:101751. https://doi.org/10.1016/j.smim.2023.101751
22. Urban CF, Nett JE. 2019. Neutrophil extracellular traps in fungal infection. Semin Cell Dev Biol 89:47–57. https://doi.org/10.1016/j.semcdb.2018.03.020
23. da Silva Dantas A, Lee KK, Raziunaite I, Schaefer K, Wagener J, Yadav B, Gow NA. 2016. Cell biology of *Candida albicans*–host interactions. Curr Opin Microbiol 34:111–118. https://doi.org/10.1016/j.mib.2016.08.006
24. Jiménez-López C, Lorenz MC. 2013. Fungal immune evasion in a model host–pathogen interaction: *Candida albicans* versus macrophages. PLoS Pathog 9:e1003741. https://doi.org/10.1371/journal.ppat.1003741
25. Williams TJ, Gonzales-Huerta LE, Armstrong-James D. 2021. Fungal-induced programmed cell death. J Fungi (Basel) 7:231. https://doi.org/10.3390/jof7030231
26. Burgess TB, Condliffe AM, Elks PM. 2022. A fun-guide to innate immune responses to fungal infections. J Fungi (Basel) 8:805. https://doi.org/10.3390/jof8080805
27. Rosowski EE, Knox BP, Archambault LS, Huttenlocher A, Keller NP, Wheeler RT, Davis JM. 2018. The zebrafish as a model host for invasive fungal infections. J Fungi (Basel) 4:136. https://doi.org/10.3390/jof4040136
28. Tobin DM, May RC, Wheeler RT. 2012. Zebrafish: a see-through host and a fluorescent toolbox to probe host–pathogen interaction. PLoS Pathog 8:e1002349. https://doi.org/10.1371/journal.ppat.1002349
29. Bergeron AC, Barker SE, Brothers KM, Prasad BC, Wheeler RT. 2017. Polyclonal anti-*Candida* antibody improves phagocytosis and overall outcome in zebrafish model of disseminated candidiasis. Dev Comp Immunol 68:69–78. https://doi.org/10.1016/j.dci.2016.11.017
30. Brothers KM, Gratacap RL, Barker SE, Newman ZR, Norum A, Wheeler RT. 2013. NADPH oxidase-driven phagocyte recruitment controls *Candida albicans* filamentous growth and prevents mortality. PLoS Pathog 9:e1003634. https://doi.org/10.1371/journal.ppat.1003634
31. Noble SM, French S, Kohn LA, Chen V, Johnson AD. 2010. Systematic screens of a *Candida albicans* homozygous deletion library decouple morphogenetic switching and pathogenicity. Nat Genet 42:590–598. https://doi.org/10.1038/ng.605
32. Lewis LE, Bain JM, Lowes C, Gillespie C, Rudkin FM, Gow NAR, Erwig L-P. 2012. Stage specific assessment of *Candida albicans* phagocytosis by macrophages identifies cell wall composition and morphogenesis as key determinants. PLoS Pathog 8:e1002578. https://doi.org/10.1371/journal.ppat.1002578
33. Mallick EM, Bergeron AC, Jones Jr SK, Newman ZR, Brothers KM, Creton R, Wheeler RT, Bennett RJ. 2016. Phenotypic plasticity regulates *Candida albicans* interactions and virulence in the vertebrate host. Front Microbiol 7:780. https://doi.org/10.3389/fmicb.2016.00780
34. Braun BR, Head WS, Wang MX, Johnson AD. 2000. Identification and characterization of TUP1-regulated genes in *Candida albicans*. Genetics 156:31–44. https://doi.org/10.1093/genetics/156.1.31
35. Gómez-Gaviria M, Vargas-Macías AP, García-Carnero LC, Martínez-Duncker I, Mora-Montes HM. 2021. Role of protein glycosylation in interactions of medically relevant fungi with the host. J Fungi (Basel) 7:875. https://doi.org/10.3390/jof7100875
36. Jia L-J, González K, Orasch T, Schmidt F, Brakhage AA. 2024. Manipulation of host phagocytosis by fungal pathogens and therapeutic opportunities. Nat Microbiol 9:2216–2231. https://doi.org/10.1038/s41564-024-01780-0
37. Uhl MA, Biery M, Craig N, Johnson AD. 2003. Haploinsufficiency-based large-scale forward genetic analysis of filamentous growth in the diploid human fungal pathogen *C.albicans*. EMBO J 22:2668–2678. https://doi.org/10.1093/emboj/cdg256
38. Cohen J. 1988. Statistical power analysis for the behavioral sciences. Routledge, New York.
39. Mao Y, Solis NV, Filler SG, Mitchell AP. 2023. Functional dichotomy for a hyphal repressor in *Candida albicans*. mBio 14:e0013423. https://doi.org/10.1128/mbio.00134-23
40. Sharma A, Mitchell AP. 2023. Strain variation in gene expression impact of hyphal cyclin Hgc1 in *Candida albicans*. G3 (Bethesda) 13:jkad151. https://doi.org/10.1093/g3journal/jkad151
41. Solis NV, Wakade RS, Glazier VE, Ollinger TL, Wellington M, Mitchell AP, Filler SG, Krysan DJ. 2022. Systematic genetic interaction analysis identifies a transcription factor circuit required for oropharyngeal candidiasis. mBio 13:e0344721. https://doi.org/10.1128/mbio.03447-21
42. Bergeron AC, Seman BG, Hammond JH, Archambault LS, Hogan DA, Wheeler RT. 2017. *Candida albicans* and *Pseudomonas aeruginosa* interact to enhance virulence of mucosal infection in transparent zebrafish. Infect Immun 85:e00475-17. https://doi.org/10.1128/IAI.00475-17
43. Bain JM, Louw J, Lewis LE, Okai B, Walls CA, Ballou ER, Walker LA, Reid D, Munro CA, Brown AJP, Brown GD, Gow NAR, Erwig LP. 2014. *Candida albicans* hypha formation and mannan masking of β-glucan inhibit macrophage phagosome maturation. mBio 5:e01874. https://doi.org/10.1128/mBio.01874-14
44. Cleary IA, Lazzell AL, Monteagudo C, Thomas DP, Saville SP. 2012. *BRG1* and *NRG1* form a novel feedback circuit regulating *Candida albicans* hypha formation and virulence. Mol Microbiol 85:557–573. https://doi.org/10.1111/j.1365-2958.2012.08127.x
45. Du H, Guan G, Xie J, Sun Y, Tong Y, Zhang L, Huang G. 2012. Roles of *Candida albicans* Gat2, a GATA-type zinc finger transcription factor, in biofilm formation, filamentous growth and virulence. PLoS One 7:e29707. https://doi.org/10.1371/journal.pone.0029707
46. Thomas G, Bain JM, Budge S, Brown AJP, Ames RM. 2020. Identifying *Candida albicans* gene networks involved in pathogenicity. Front Genet 11:375. https://doi.org/10.3389/fgene.2020.00375
47. Lopes JP, Lionakis MS. 2022. Pathogenesis and virulence of *Candida albicans*. Virulence 13:89–121. https://doi.org/10.1080/21505594.2021.2019950
48. Ferrigno P, Posas F, Koepp D, Saito H, Silver PA. 1998. Regulated nucleo/cytoplasmic exchange of HOG1 MAPK requires the importin beta homologs NMD5 and XPO1. EMBO J 17:5606–5614. https://doi.org/10.1093/emboj/17.19.5606
49. Polizotto RS, Cyert MS. 2001. Calcineurin-dependent nuclear import of the transcription factor Crz1p requires Nmd5p. J Cell Biol 154:951–960. https://doi.org/10.1083/jcb.200104078
50. Quan X, Rassadi R, Rabie B, Matusiewicz N, Stochaj U. 2004. Regulated nuclear accumulation of the yeast hsp70 Ssa4p in ethanol-stressed cells is mediated by the N-terminal domain, requires the nuclear carrier Nmd5p and protein kinase C. FASEB J 18:899–901. https://doi.org/10.1096/fj.03-0947fje
51. Hall CJ, Boyle RH, Astin JW, Flores MV, Oehlers SH, Sanderson LE, Ellett F, Lieschke GJ, Crosier KE, Crosier PS. 2013. *Immunoresponsive gene* 1 augments bactericidal activity of macrophage-lineage cells by regulating β-oxidation-dependent mitochondrial ROS production. Cell Metab 18:265–278. https://doi.org/10.1016/j.cmet.2013.06.018
52. Scherer AK, Blair BA, Park J, Seman BG, Kelley JB, Wheeler RT. 2020. Redundant Trojan horse and endothelial-circulatory mechanisms for host-mediated spread of *Candida albicans* yeast. PLoS Pathog 16:e1008414. https://doi.org/10.1371/journal.ppat.1008414
53. Gervais NC, Halder V, Shapiro RS. 2021. A data library of *Candida albicans* functional genomic screens. FEMS Yeast Res 21:foab060. https://doi.org/10.1093/femsyr/foab060
54. Witchley JN, Penumetcha P, Abon NV, Woolford CA, Mitchell AP, Noble SM. 2019. *Candida albicans* morphogenesis programs control the balance between gut commensalism and invasive infection. Cell Host Microbe 25:432–443. https://doi.org/10.1016/j.chom.2019.02.008
55. Brothers KM, Wheeler RT. 2012. Non-invasive imaging of disseminated candidiasis in zebrafish larvae. J Vis Exp:4051. https://doi.org/10.3791/4051
56. Bai C, Ramanan N, Wang YM, Wang Y. 2002. Spindle assembly checkpoint component CaMad2p is indispensable for *Candida albicans* survival and virulence in mice. Mol Microbiol 45:31–44. https://doi.org/10.1046/j.1365-2958.2002.02995.x
57. Csank C, Schröppel K, Leberer E, Harcus D, Mohamed O, Meloche S, Thomas DY, Whiteway M. 1998. Roles of the *Candida albicans* mitogen-activated protein kinase homolog, Cek1p, in hyphal development and systemic candidiasis. Infect Immun 66:2713–2721. https://doi.org/10.1128/IAI.66.6.2713-2721.1998
58. Davis D, Edwards Jr JE, Mitchell AP, Ibrahim AS. 2000. *Candida albicans* RIM101 pH response pathway is required for host-pathogen interactions. Infect Immun 68:5953–5959. https://doi.org/10.1128/IAI.68.10.5953-5959.2000
59. Gratacap RL, Rawls JF, Wheeler RT. 2013. Mucosal candidiasis elicits NF-κB activation, proinflammatory gene expression and localized neutrophilia in zebrafish. Dis Model Mech 6:1260–1270. https://doi.org/10.1242/dmm.012039

60. O'Meara TR, O'Meara MJ. 2021. DeORFanizing *Candida albicans* genes using coexpression. mSphere 6:e01245-20. https://doi.org/10.1128/mSphere.01245-20
61. Castrejon F, Gomez A, Sanz M, Duran A, Roncero C. 2006. The RIM101 pathway contributes to yeast cell wall assembly and its function becomes essential in the absence of mitogen-activated protein kinase Slt2p. Eukaryot Cell 5:507–517. https://doi.org/10.1128/EC.5.3.507-517.2006
62. Nobile CJ, Solis N, Myers CL, Fay AJ, Deneault JS, Nantel A, Mitchell AP, Filler SG. 2008. *Candida albicans* transcription factor Rim101 mediates pathogenic interactions through cell wall functions. Cell Microbiol 10:2180–2196. https://doi.org/10.1111/j.1462-5822.2008.01198.x
63. Petit J, Bailey EC, Wheeler RT, de Oliveira CAF, Forlenza M, Wiegertjes GF. 2019. Studies into β-glucan recognition in fish suggests a key role for the C-type lectin pathway. Front Immunol 10:280. https://doi.org/10.3389/fimmu.2019.00280
64. Brenes LR, Lohse MB, Hartooni N, Johnson AD. 2020. A set of diverse genes influence the frequency of white-opaque switching in *Candida albicans*. G3 (Bethesda) 10:2593–2600. https://doi.org/10.1534/g3.120.401249
65. Enjalbert B, Smith DA, Cornell MJ, Alam I, Nicholls S, Brown AJP, Quinn J. 2006. Role of the Hog1 stress-activated protein kinase in the global transcriptional response to stress in the fungal pathogen *Candida albicans*. Mol Biol Cell 17:1018–1032. https://doi.org/10.1091/mbc.e05-06-0501
66. Kämmer P, McNamara S, Wolf T, Conrad T, Allert S, Gerwien F, Hünniger K, Kurzai O, Guthke R, Hube B, Linde J, Brunke S. 2020. Survival strategies of pathogenic *Candida* species in human blood show independent and specific adaptations. mBio 11:e02435-20. https://doi.org/10.1128/mBio.02435-20
67. Niemiec MJ, Grumaz C, Ermert D, Desel C, Shankar M, Lopes JP, Mills IG, Stevens P, Sohn K, Urban CF. 2017. Dual transcriptome of the immediate neutrophil and *Candida albicans* interplay. BMC Genomics 18:696. https://doi.org/10.1186/s12864-017-4097-4
68. Nobile CJ, Fox EP, Nett JE, Sorrells TR, Mitrovich QM, Hernday AD, Tuch BB, Andes DR, Johnson AD. 2012. A recently evolved transcriptional network controls biofilm development in *Candida albicans*. Cell 148:126–138. https://doi.org/10.1016/j.cell.2011.10.048
69. Pountain AW, Collette JR, Farrell WM, Lorenz MC. 2021. Interactions of both pathogenic and nonpathogenic CUG clade *Candida* species with macrophages share a conserved transcriptional landscape. mBio 12:e0331721. https://doi.org/10.1128/mbio.03317-21
70. Wang JM, Woodruff AL, Dunn MJ, Fillinger RJ, Bennett RJ, Anderson MZ. 2021. Intraspecies transcriptional profiling reveals key regulators of *Candida albicans* pathogenic traits. mBio 12:e00586-21. https://doi.org/10.1128/mBio.00586-21
71. Dalal CK, Zuleta IA, Mitchell KF, Andes DR, El-Samad H, Johnson AD. 2016. Transcriptional rewiring over evolutionary timescales changes quantitative and qualitative properties of gene expression. Elife 5:e18981. https://doi.org/10.7554/eLife.18981
72. Nocedal I, Mancera E, Johnson AD. 2017. Gene regulatory network plasticity predates a switch in function of a conserved transcription regulator. Elife 6:e23250. https://doi.org/10.7554/eLife.23250
73. Reuss O, Vik A, Kolter R, Morschhäuser J. 2004. The *SAT1* flipper, an optimized tool for gene disruption in *Candida albicans*. Gene 341:119–127. https://doi.org/10.1016/j.gene.2004.06.021
74. Moyes DL, Wilson D, Richardson JP, Mogavero S, Tang SX, Wernecke J, Höfs S, Gratacap RL, Robbins J, Runglall M, et al. 2016. Candidalysin is a fungal peptide toxin critical for mucosal infection. Nature 532:64–68. https://doi.org/10.1038/nature17625
75. Peters BM, Palmer GE, Nash AK, Lilly EA, Fidel Jr PL, Noverr MC. 2014. Fungal morphogenetic pathways are required for the hallmark inflammatory response during *Candida albicans* vaginitis. Infect Immun 82:532–543. https://doi.org/10.1128/IAI.01417-13
76. Seman BG, Moore JL, Scherer AK, Blair BA, Manandhar S, Jones JM, Wheeler RT. 2018. Yeast and filaments have specialized, independent activities in a zebrafish model of *Candida albicans* infection. Infect Immun 86:e00415-18. https://doi.org/10.1128/IAI.00415-18
77. Wu Y, Du S, Johnson JL, Tung HY, Landers CT, Liu Y, Seman BG, Wheeler RT, Costa-Mattioli M, Kheradmand F, Zheng H, Corry DB. 2019. Microglia and amyloid precursor protein coordinate control of transient *Candida* cerebritis with memory deficits. Nat Commun 10:58. https://doi.org/10.1038/s41467-018-07991-4
78. Ellett F, Pase L, Hayman JW, Andrianopoulos A, Lieschke GJ. 2011. *mpeg1* promoter transgenes direct macrophage-lineage expression in zebrafish. Blood 117:e49–56. https://doi.org/10.1182/blood-2010-10-314120
79. Hall C, Flores MV, Storm T, Crosier K, Crosier P. 2007. The zebrafish lysozyme C promoter drives myeloid-specific expression in transgenic fish. BMC Dev Biol 7:42. https://doi.org/10.1186/1471-213X-7-42
80. de Oliveira S, Lopez-Muñoz A, Martínez-Navarro FJ, Galindo-Villegas J, Mulero V, Calado Â. 2015. Cxcl8-l1 and Cxcl8-l2 are required in the zebrafish defense against *Salmonella* Typhimurium. Dev Comp Immunol 49:44–48. https://doi.org/10.1016/j.dci.2014.11.004
81. Nguyen-Chi M, Laplace-Builhe B, Travnickova J, Luz-Crawford P, Tejedor G, Phan QT, Duroux-Richard I, Levraud JP, Kissa K, Lutfalla G, Jorgensen C, Djouad F. 2015. Identification of polarized macrophage subsets in zebrafish. Elife 4:e07288. https://doi.org/10.7554/eLife.07288
82. Mattingly CJ, Hampton TH, Brothers KM, Griffin NE, Planchart A. 2009. Perturbation of defense pathways by low-dose arsenic exposure in zebrafish embryos. Environ Health Perspect 117:981–987. https://doi.org/10.1289/ehp.0900555
83. Quinn GP, Keough MJ. 2002. Experimental design and data analysis for biologists. Cambridge University Press.
84. Hedges LV, Olkin O. 1985. Statistical methods for meta-analysis. Academic Press.
85. Council NR. 2011. Guide for the care and use of laboratory animals. National Academies Press, Washington, D.C.